Efficient reduction for diagnosing Hopf bifurcation in delay differential systems: Applications to cloud-rain models

Cite as: Chaos **30**, 053130 (2020); https://doi.org/10.1063/5.0004697
Submitted: 13 February 2020 . Accepted: 23 April 2020 . Published Online: 15 May 2020

Mickaël D. Chekroun, Ilan Koren, and Honghu Liu

Efficient reduction for diagnosing Hopf bifurcation in delay differential systems: Applications to cloud-rain models

Cite as: Chaos **30**, 053130 (2020); doi: 10.1063/5.0004697
Submitted: 13 February 2020 · Accepted: 23 April 2020 ·
Published Online: 15 May 2020

Mickaël D. Chekroun,[1,2,a)] Ilan Koren,[1,b)] and Honghu Liu[3,c)]

AFFILIATIONS

[1]Department of Earth and Planetary Sciences, Weizmann Institute, Rehovot 76100, Israel
[2]Department of Atmospheric and Oceanic Sciences, University of California, Los Angeles, Los Angeles, California 90095-1565, USA
[3]Department of Mathematics, Virginia Tech, Blacksburg, Virginia 24061, USA

[a)]**Author to whom correspondence should be addressed:** michael-david.chekroun@weizmann.ac.il
[b)]ilan.koren@weizmann.ac.il
[c)]hhliu@vt.edu

ABSTRACT

By means of Galerkin–Koornwinder (GK) approximations, an efficient reduction approach to the Stuart–Landau (SL) normal form and center manifold is presented for a broad class of nonlinear systems of delay differential equations that covers the cases of discrete as well as distributed delays. The focus is on the Hopf bifurcation as a consequence of the critical equilibrium's destabilization resulting from an eigenpair crossing the imaginary axis. The nature of the resulting Hopf bifurcation (super- or subcritical) is then characterized by the inspection of a Lyapunov coefficient easy to determine based on the model's coefficients and delay parameters. We believe that our approach, which does not rely too much on functional analysis considerations but more on analytic calculations, is suitable to concrete situations arising in physics applications. Thus, using this GK approach to the Lyapunov coefficient and the SL normal form, the occurrence of Hopf bifurcations in the cloud-rain delay models of Koren and Feingold (KF) on one hand and Koren, Tziperman, and Feingold on the other are analyzed. Noteworthy is the existence of the KF model of large regions of the parameter space for which subcritical and supercritical Hopf bifurcations coexist. These regions are determined, in particular, by the intensity of the KF model's nonlinear effects. "Islands" of supercritical Hopf bifurcations are shown to exist within a subcritical Hopf bifurcation "sea"; these islands being bordered by double-Hopf bifurcations occurring when the linearized dynamics at the critical equilibrium exhibit two pairs of purely imaginary eigenvalues.

A new approach to analyze and detect Hopf bifurcations in nonlinear systems of delay differential equations (DDEs) is proposed. By means of Galerkin approximations, the DDEs are reduced to ordinary differential equations (ODEs). An efficient reduction approach to the Stuart–Landau (SL) oscillators and center manifold is then presented for a broad class of nonlinear systems of DDEs that covers the cases of discrete and distributed delays. The nature of the resulting Hopf bifurcation (super- or subcritical) is then characterized by the inspection of a Lyapunov coefficient easy to determine based on the model's coefficients and delay parameters. Applications to cloud-rain models are discussed in detail. New dynamical behaviors are exhibited for these models such as double-Hopf bifurcations, and new dynamical insights about the physical regimes are discussed.

I. INTRODUCTION

The characterization of Hopf bifurcations for delay differential equations (DDEs) has been extensively analyzed. A widely adopted approach consists of first reducing the given DDE to a low-dimensional ordinary differential equation (ODE) system by combining center-manifold reduction with a normal form theory for ODEs, either consecutively (e.g., Ref. 1) or simultaneously (e.g., Ref. 2); see also Refs. 3–6. Other approaches include the method of averaging,[7] topological methods,[8] the Fredholm alternative,[9] the Lyapunov–Schmidt method,[10] or the method of multiple scales.[11,12] A review of the Hopf bifurcation theory for DDE systems is available in Refs. 13 and 14. For normal form calculations and reduction to center manifolds for DDEs, we refer to Chap. 8 in Ref. 15, and to

Ref. 4 (relying on the earlier work[16]) for the first closed-form Hopf bifurcation calculation, carried out for scalar nonlinear DDEs; see Ref. 17 for systems of DDEs.

Whatever the approach retained, the specific type of Hopf bifurcation depends on certain analytic conditions, which involve nonlinearities from the equations, and conditions that may turn out to be tricky to check in practice. Because of the complexity of calculations, computer algebra programs are often used for detecting and analyzing Hopf bifurcations in DDEs.[5,18–20] We mention also the versatile DDE-BIFTOOL Matlab package[21–24] for the numerical bifurcation analysis of systems of DDEs, which allows for the numerical continuation of branches of stable and unstable orbits against the chosen bifurcation parameters. The pseudospectral methods of Ref. 25 used to derive ODE approximations and to analyze from them the stability and bifurcation of equilibria of the original DDE model by available software packages for continuation and bifurcation for ODEs are also another useful approach.

In this article, we propose a new approach based on the Galerkin–Koornwinder (GK) method introduced in Ref. 26, which leads to simple analytic conditions to verify in practice for characterizing the type of Hopf bifurcation. As shown in Ref. 26, Koornwinder polynomials[27] (see Appendix A) allow for rigorous approximation by ODEs of a broad class of nonlinear systems of DDEs, including the case of discrete delays, distributed delays, and multiple delays; see also Sec. II B. We refer to Ref. 26 for a detailed discussion about the difference between the GK method and other Galerkin techniques for DDEs. Aside from the rigorous aspects of the GK approach, the GK method has shown to bring analytical insights useful for other applications than bifurcations for DDEs. For instance, the GK approach has demonstrated its efficiency for the optimal control of nonlinear DDEs,[28] making affordable numerically the computation of (nearly) optimal controls in a feedback form from the corresponding approximations of the infinite-dimensional Hamilton–Jacobi–Bellman equation. An important ingredient provided by the GK approach for such accomplishments lies in the explicit dependence on the delay parameter (or, more generally, distributed delays[26]) that appears in the coefficients of the GK approximations rather than through arguments of the state variable as for DDEs.

In this article, we propose to further explore the capabilities of the GK approach in the context of Hopf bifurcations. As shown hereafter, the analytical insights provided by the GK method allow for extracting reduced coordinates via its combination with center-manifold techniques; see, in that respect, Sec. III C. Essentially, the idea consists of applying the center-manifold reduction to a GK ODE approximation rather than to the original DDE system. This reduction is then followed by an elimination of the non-determining nonlinear terms (i.e., the non-resonant terms) by using the normal form theory; see the proof of Theorem III.1 in Appendix A 5. Thanks to the rigorous convergence results of Ref. 26, it is legitimate to argue that a Hopf bifurcation, along with its type (super- or subcritical), which occurs in the DDE dynamics, is actually captured both qualitatively and quantitatively by a sufficiently high-dimensional GK approximation.

In that respect, given a nonlinear DDE system, Theorem III.1 provides a characterization of Hopf bifurcations occurring in a GK approximation (28) of this DDE system. It is shown that this characterization boils down essentially to (i) the computation of eigenvalues and eigenvectors of the matrix Γ_N in (28) and its adjoint Γ_N^*, involving the model's coefficients and delay parameters, and to (ii) the computation of inner products; see (38)–(40). Such a characterization is made possible by reducing analytically the GK system into a two-dimensional normal form, which turns out to be a Stuart–Landau (SL) equation as classically encountered in the normal form theory of Hopf bifurcations.[29,30] The originality of our treatment lies in the details about the coefficients of this equation; see Eq. (36). Such analytic formulas for the corresponding Stuart–Landau (SL) equation (Theorem III.1) are especially useful for the modeling/analysis of multiscale datasets exploiting SL equations.[31–35]

We mention indeed that Theorem III.1 presents its own interest outside of the scope of ODE approximations to DDE systems. The characterization of Hopf bifurcations for high-dimensional ODE systems by using center-manifold (CM) reduction is known (Ref. 36, pp. 110–114), but the formulas are typically involved, as derived directly from the reduced equations on the center-manifold without exploiting approximations to CM. The leading-order approximation formulas of invariant manifolds such as derived in Theorem 2 of Ref. 37 form the cornerstone of our treatment of this problem; see Appendix A 5. The resulting Theorem III.1 shows that these formulas are sufficient to characterize Hopf bifurcations by determining exactly the Lyapunov coefficient.

We were not able to find in the recent literature the explicit dependence on the nonlinear effects of the Lyapunov coefficient formula (40) such as provided by Theorem III.1. Such a formula appears in an often convoluted fashion for high-dimensional systems [Eqs. (3.18), (3.19), and (5.32) in Ref. 30], without the nonlinear effect dependences made transparent with the few coefficients listed in (38) and (39) hereafter. We emphasize that for Galerkin approximations of DDE systems, these formulas are anyway new.

The study of delayed effects and mechanisms is rising in climate modeling (see Refs. 38–41 and references therein), but only recently, the analysis of the corresponding DDE model's bifurcations or transitions has been undertaken; see, e.g., Refs. 42–47 for delay models concerned with the El Niño-Southern Oscillation. We refer to Ref. 48 for a general introduction about the role of delays such as arising in biological models, engineering applications, and mechanics. Recently, delay models have been proposed as elemental cloud physics models.[49,50] The analysis of the bifurcations arising in these models is still in its infancy. To advance this analysis, Sec. IV provides applications of the theory presented in this article to the Koren–Feingold (KF) cloud-rain model.[49] Applications to the simpler Koren, Tziperman, and Feingold (KTF) model[50] are shown in Sec. III B. The cloud and rain nonlinear system of DDEs in Ref. 49 describes the interplay between recharging the cloud water driven by the environmental instability (parametrized by the boundary layer thickness and speed of recharging) and the cloud discharge by rain. The delay parametrizes the time it takes from the onset of droplet coalesce to the rain sedimentation. The KF model is described by a set of two coupled DDEs: one for the time evolution of cloud thickness and the other one for the aerosol concentration that dictates the droplet concentration and is scavenged by the rain. The KTF simplified model is formulated as only one scalar nonlinear DDE for the

cloud thickness letting the aerosol concentration to be a constant free parameter of the environment.

Using the proposed GK approach, we analyze the occurrence of Hopf bifurcations in both the KTF model and the KF model. In particular, we found that for the KF model, there are broad regions of the parameter space for which subcritical and supercritical Hopf bifurcations coexist, whose nature is characterized by the interactions of linearized modes through the KF model's nonlinear terms. Supercritical Hopf bifurcations are characterized by the emergence of stable limit cycles, while the subcritical one, by the emergence of unstable limit cycles. Each type of periodic solutions is found numerically in the KF model for physical parameter regimes such as considered in Ref. 49; see Sec. IV D. By varying the intensity of the KF model's nonlinear effects, we found "islands" of supercritical Hopf bifurcations within a subcritical Hopf bifurcation "sea"; and at the supercritical/subcritical boundary, double-Hopf bifurcations can occur when the linearized dynamics at the critical equilibrium exhibit two pairs of eigenvalues sitting on the imaginary axis; see Fig. 9. For a better reproducibility of the results, practical details about the analytic treatment of the Lyapunov coefficient are provided in Appendix B, while details about our numerical implementations are provided in Appendix C.

This article is organized as follows. In Sec. II, we revisit the analytical aspects for the derivation of GK approximations of nonlinear DDE systems such as found in Ref. 26. In Sec. III, the Hopf bifurcation-characterization theorem is formulated for such GK approximations (Theorem III.1), and in particular, an analytic formula of the Lyapunov coefficient is provided; see (40). Then, applications to the KTF model are discussed in Sec. III B, while an explicit calculation and visualization of the leading-approximation to the center manifold are performed in Sec. III C. Applications to the KF model are discussed in Sec. IV. Appendixes A–C present finally some key technical details about Koornwinder polynomials for GK approximations, the calculation of the Lyapunov coefficient, and numerical implementation aspects, respectively.

II. ODE APPROXIMATION OF DDE SYSTEMS: THE GALERKIN–KOORNWINDER (GK) METHOD

A. The GK method: The first intuition

Let us first recall some useful interpretations about DDEs in view of outlining the main ideas behind the GK method. To serve our purpose, we consider the following model taken from Ref. 50:

$$\frac{\mathrm{d}h}{\mathrm{d}t} = 1 + ah(t) - bh^2(t-\tau), \quad \tau > 0; \tag{1}$$

see Eq. (3) in Ref. 50 in which $a = -1$ and $b = \frac{1}{\mu}$. Here, the variable h corresponds to the normalized height of the cloud.

We recall that in order to describe the solution to a DDE such as (1), it is classical to distinguish between the *historic part* of the evolving state, $\{h(t+\theta) : \theta \in [-\tau, 0)\}$, and its *current state*, $h(t)$.

Denoting by $u(t,\theta)$ the historic part, one then rewrites the DDE (1) as the transport equation,

$$\partial_t u = \partial_\theta u, \quad -\tau \le \theta < 0, \tag{2}$$

subject to the *nonlocal and nonlinear boundary condition*,

$$\begin{aligned}\partial_\theta u|_{\theta=0} &= 1 + au(t,0) - bu^2(t,-\tau)\\ &= au(t,0) + F(u(t,-\tau)), \quad t \ge 0.\end{aligned} \tag{3}$$

The theory presented in Ref. 26 allows for handling much more general situations, but we use this simple example here to give a sense of the main ideas, namely, the strategy adopted to approximate this nonlocal boundary problem by a set of ODEs. To do so, we take our phase space $\mathcal{X}$ to be $L^2([-\tau,0),\mathbb{R})$, the space of square integrable functions on $[-\tau,0)$. It means that we want to recast the nonlocal boundary problem (2) and (3) into an abstract ODE whose solutions are described by functions that lie in $\mathcal{X}$. Due to the nonlocal character of the boundary condition, we work actually within the extended phase space $\mathcal{H} = \mathcal{X} \times \mathbb{R}$.

More precisely, by introducing, $U(t) = (u(t,\cdot), u(t,0))$, the nonlocal boundary problem (2) and (3) is then recast into the following infinite-dimensional ODE posed in $\mathcal{H}$,

$$\frac{\mathrm{d}U}{\mathrm{d}t} = AU + X_0 F(u(t,-\tau)), \quad U \in \mathcal{H}, \tag{4}$$

with $F(x) = 1 - bx^2$, and

$$AU = \partial_\theta u(t,\theta) + X_0(au(t,0) - \partial_\theta u|_{\theta=0}), \tag{5}$$

where

$$X_0 = \begin{cases} 0, & \theta \in [-\tau, 0), \\ 1, & \theta = 0. \end{cases} \tag{6}$$

To make sense of Eq. (4), i.e., to have existence and uniqueness, the solutions $U(t)$ are sought in a subspace $\mathcal{V}$ of $\mathcal{H}$, which imposes the following constraints on $U(t)$ that for all t,[26]

$$u(t,\theta) \in H^1([-\tau,0);\mathbb{R}), \text{ and } \lim_{\theta\to 0^-} u(t,\theta) = u(t,0). \tag{7}$$

Here given a dimension d of the current state, the space, $H^1([-\tau,0);\mathbb{R}^d)$ denotes the standard Sobolev subspace of $L^2([-\tau,0);\mathbb{R}^d)$; see, e.g., Chap. 8 in Ref. 51. This space consists of functions that are square integrable and whose first-order weak derivatives exist in a distributional sense and are also square integrable. Note that $H^1([-\tau,0);\mathbb{R}^d)$ is continuously embedded in the space of continuous functions $C([-\tau,0];\mathbb{R}^d)$; see Theorem 8.8 of Ref. 51. The solutions we are manipulating throughout this article are thus, in particular, continuous but not necessarily with a continuous derivative.

In other words, $\mathcal{V}$ is the following subspace of functions $\psi = (\phi, x)$ of $\mathcal{H}$:

$$\mathcal{V} = \{\psi \in \mathcal{H} : \phi \in H^1([-\tau,0);\mathbb{R}), \text{ and } \lim_{\theta\to 0^-} \phi(\theta) = x\}. \tag{8}$$

Mathematically, the subspace $\mathcal{V}$ is the domain of the linear operator A, which means that $A\phi$ is well-defined for ϕ in $\mathcal{V}$; see Theorem 2.4.6 of Ref. 52.

Remark II.1: *The reframing of the (nonlinear) DDE (1) into the transport equation (2) subject to the nonlocal (and nonlinear) boundary condition (3) is depicted by the schematic of Fig. 1. It also emphasizes that a DDE such as (1) must be initiated over an initial history ϕ given on $[-\tau,0)$ and not only its point value $\phi(0)$. The existence and uniqueness of the DDE solution translates to the*

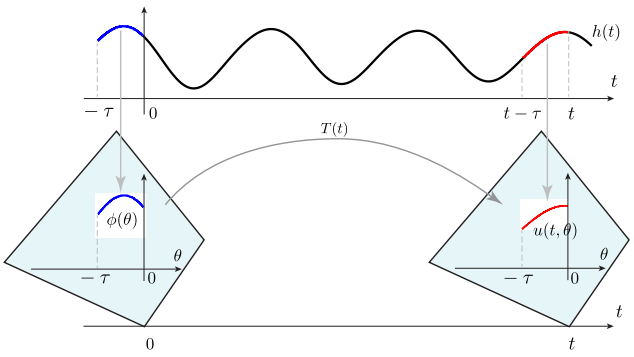

FIG. 1. Reframing the DDE (1) into the transport equation (2) subject to the nonlocal boundary condition (3). Here, it is emphasized that a DDE such as (1) must be initiated over an initial history ϕ given on $[-\tau, 0)$. The existence and uniqueness of a DDE solution translates as the existence of a nonlinear solution operator, $T(t)$, that assigns to each ϕ, a unique solution $u(t,\theta)$ to (2) and (3) at time t, namely, $u(t,\cdot) = T(t)\phi$.

existence of a nonlinear solution operator, $T(t)$, that assigns to each ϕ, a unique solution $u(t,\theta)$ to (2) and (3) at time t, namely, $u(t,\cdot) = T(t)\phi$. See Ref. 13 for an introduction to the theory of DDEs with the state space to be the space of continuous functions $C([-\tau,0];\mathbb{R}^d)$.

The idea is then (i) to find a finite-dimensional subspace $\mathcal{H}_N$ of $\mathcal{V}$, spanned by N functions φ_j (orthogonal in $\mathcal{H}$) to be defined and (ii) to find an approximation A_N of A such that $A_N\mathcal{H}_N \subset \mathcal{H}_N$, i.e., $\mathcal{H}_N$ is invariant under A_N. This way, by projecting onto $\mathcal{H}_N$, one obtains a finite-dimensional ODE approximation of Eq. (4) (a Galerkin approximation). As a by-product, by answering (i) and (ii), we find a Galerkin approximation of the nonlocal problem (2) and (3) and thus of the DDE (1).

The main contribution of Ref. 26 was to prove that the φ_j's may be obtained from the Koornwinder polynomials[27] for much more general DDEs than Eq. (1); see Sec. II B. These Koornwinder polynomials and their main properties are discussed in Appendix A 1. These polynomials originally given on $[-1,1]$ are rescaled into polynomials K_j^τ's defined on $[-\tau,0]$ (A10) to approximate solutions to, e.g., the nonlocal problem (2) and (3).

Using these rescaled Koornwinder polynomials, a solution $u(t,\theta)$ solving (2) and (3) is approximated by

$$u_N(t,\theta) = \sum_{j=0}^{N-1} y_j(t) K_j^\tau(\theta), \tag{9}$$

while $h(t) := u(t,0)$ is approximated by

$$h_N(t) = \sum_{j=0}^{N-1} y_j(t). \tag{10}$$

Note that in (9), the Koornwinder polynomials are indexed according to their degree j.

Next, we substitute U in (4) by its approximation (u_N, h_N) and project Eq. (4) onto the approximation space,

$$\mathcal{H}_N = \mathrm{span}\{\mathcal{K}_0^\tau, \ldots, \mathcal{K}_{N-1}^\tau\}, \tag{11}$$

where the $\mathcal{K}_j^\tau$'s denote the Koornwinder polynomials to which a point value has been added according to (A11) so that each $\mathcal{K}_j^\tau$ lies in the function space $\mathcal{V}$.

After calculations, we arrive at the following N-dimensional ODE approximation (Sec. 5 in Ref. 26),

$$\frac{d\boldsymbol{y}}{dt} = \left(\frac{2}{\tau}P_N + Q_N\right)\boldsymbol{y} + F_N(\boldsymbol{y}), \tag{12}$$

where P_N and Q_N are $N \times N$ matrices for which only Q_N depends on the model's parameters; see (46). The matrix P_N results from the expansion of the derivative of a given Koornwinder polynomial in terms of the others; see Sec. 5 of Ref. 26. See also Appendix A 2.

In Eq. (12), the nonlinear term F in (4) is approximated by the following nonlinear mapping [see (48)]:

$$F_N(\boldsymbol{y}) = \left(1 - b\left(\sum_{j=0}^{N-1} y_j K_j(-1)\right)^2\right)\boldsymbol{v}_N \tag{13}$$

with

$$\boldsymbol{v}_N = \left(\frac{1}{\|\mathcal{K}_0\|^2}, \ldots, \frac{1}{\|\mathcal{K}_{N-1}\|^2}\right)^{\mathrm{T}}, \tag{14}$$

where the $\mathcal{K}_j$'s denote the Koornwinder polynomials to which a point value has been added according to (A4). Note that $\|\mathcal{K}_{N-1}\|^{-2}$ decreases as N^{-3} according to (A7).

Equation (12) is called a Galerkin–Koornwinder (GK) approximation. This approximation method scales up to nonlinear systems of DDEs. Actually, in Ref. 26, the GK method was shown to provide approximations rigorously justified for a broad class of nonlinear systems of DDEs (Corollaries 4.1–4.3 in Ref. 26) and very effective in nonlinear cases that yield quasi-periodic and chaotic, as well as nearly Brownian dynamics, or for the optimal control in the feedback form[53] of nonlinear DDEs.[28] In each case, low-dimensional ODE systems succeed in approximating important topological as well as statistical features of the corresponding DDE's nonlinear dynamics. We turn next to the class of DDE systems covered by the GK method and describe the analytic approximation formulas.

B. The systems of DDEs covered

The d-dimensional nonlinear systems of DDEs considered in this article are of the following form:

$$\frac{d\mathbf{x}}{dt} = L\mathbf{x}(t) + B\mathbf{x}(t-\tau) + C\int_{t-\tau}^{t} \mathbf{x}(s)\,ds + \mathbf{F}\left(\mathbf{x}(t), \mathbf{x}(t-\tau), \int_{t-\tau}^{t} \mathbf{x}(s)\,ds\right), \tag{15}$$

where L, B, and C are $d \times d$ matrices and $\mathbf{F}: \mathbb{R}^d \times \mathbb{R}^d \times \mathbb{R}^d \to \mathbb{R}^d$ is a nonlinear function such that (15) is well-posed in $\mathcal{H}_d = L^2([-\tau,0);\mathbb{R}^d) \times \mathbb{R}^d$, after recasting the system (15) into an abstract ODE.

Our goal is to derive rigorous results about Hopf bifurcations for GK approximations and to relate these results to the original system (15). In particular, the derivation of normal forms to GK approximations of (15) along with a simple criterion to characterize whether a Hopf bifurcation is subcritical or supercritical is one of the main focuses of this article.

C. The GK method: Analytic formulas of approximation

Following Ref. 26, to approximate nonlinear systems of DDEs such as (15), we use vectorized version, $\mathbb{K}_j^\tau$, of Koornwinder polynomials such as described in Appendix A 3; see (A25).

The finite-dimensional GK approximations of the DDE system (15) are based on a reformulation of (15) into an infinite-dimensional ODE (followed by the projection on a subspace spanned by Koornwinder polynomials) in the same way as explained in Sec. II A for the example (1). This reformulation concerns the new variable $U(t,\theta) = (u(t,\theta), u(t,0))$, where, as before, $u(t,\theta) = \mathbf{x}(t+\theta)$ for θ in $[-\tau,0)$, denotes the historical segment and $u(t,0) = \mathbf{x}(t)$ is the current state. The state space for U is the Hilbert space $\mathcal{H}_d = L^2([-\tau,0);\mathbb{R}^d) \times \mathbb{R}^d$.

In a similar fashion than in Sec. II A, we thus first recast the DDE system (15) into an abstract, infinite-dimensional, ODE posed in $\mathcal{H}_d$. To do so, the nonlinear effects are recast into the following mapping acting on $\psi = (\phi, x)$ in $\mathcal{H}_d$:

$$[\mathcal{F}(\psi)](\theta) = \begin{cases} 0, & \theta \in [-\tau,0), \\ \mathbf{F}\left(x, \phi(-\tau), \int_{-\tau}^0 \phi(s)\,\mathrm{d}s\right), & \theta = 0, \end{cases} \tag{16}$$

while the linear part becomes

$$[\mathcal{A}\psi](\theta) = \begin{cases} \dfrac{\mathrm{d}\psi}{\mathrm{d}\theta}, & \theta \in [-\tau,0), \\ L x + B\phi(-\tau) + C\int_{-\tau}^0 \phi(s)\,\mathrm{d}s, & \theta = 0. \end{cases} \tag{17}$$

We have then that $U(t,\theta) = (\mathbf{x}(t+\theta), \mathbf{x}(t))$ satisfies

$$\frac{\mathrm{d}U}{\mathrm{d}t} = \begin{cases} \frac{\mathrm{d}\mathbf{x}(t+\theta)}{\mathrm{d}\theta}, & \theta \in [-\tau,0), \\ L\mathbf{x}(t) + B\mathbf{x}(t-\tau) + C\int_{-\tau}^0 \mathbf{x}(t+s)\,\mathrm{d}s + \mathbf{F}\left(\mathbf{x}(t), \mathbf{x}(t-\tau), \int_{-\tau}^0 \mathbf{x}(t+s)\,\mathrm{d}s\right), & \theta = 0, \end{cases} \tag{18}$$

that is,

$$\frac{\mathrm{d}U}{\mathrm{d}t} = \mathcal{A}U + \mathcal{F}(U), \quad U \in \mathcal{H}_d. \tag{19}$$

Given the reduced state space,

$$\mathcal{H}_N = \mathrm{span}\left\{\mathbb{K}_1^\tau, \ldots, \mathbb{K}_{Nd}^\tau\right\} \subset \mathcal{H}_d, \tag{20}$$

spanned by the first Nd (vectorized) Koornwinder polynomials, the Galerkin approximation of (19) takes then the form

$$\frac{\mathrm{d}U_N}{\mathrm{d}t} = \Pi_N \mathcal{A}\Pi_N U_N + \Pi_N \mathcal{F}(U_N), \tag{21}$$

where Π_N denotes the projector onto $\mathcal{H}_N$. Note that the choice of Koornwinder polynomials makes

$$\mathcal{A}_N\psi = \Pi_N\mathcal{A}\Pi_N\psi, \quad \psi \in \mathcal{H}_d, \tag{22}$$

well defined on $\mathcal{H}_d$; i.e., $\Pi_N\psi$ belongs to the domain of $\mathcal{A}$ for any ψ in $\mathcal{H}_d$; see Ref. 26. The properties of Koornwinder polynomials recalled in Appendix A allow us for obtaining an analytic expression of $\mathcal{A}_N$ and thus of the Galerkin approximation Eq. (21); see Eq. (26). We outline below the main outcomes of these calculations and refer to Appendix A 4 for more details.

To do so, note first that given any initial datum U_0 in $\mathcal{H}_N$, the corresponding solution U_N to Eq. (21) has the following expansion:

$$U_N(t,\theta) = \sum_{n=1}^{Nd} y_n(t)\mathbb{K}_n^\tau(\theta), \quad \theta \in [-\tau,0), \tag{23}$$

where

$$y_n(t) = \frac{\langle U_N(t,\cdot), \mathbb{K}_n^\tau\rangle_{\mathcal{H}_d}}{\|\mathbb{K}_n^\tau\|_{\mathcal{H}_d}^2}. \tag{24}$$

Now, replacing U_N in Eq. (21) by its expansion (23) and taking the $\mathcal{H}_d$-inner product on both sides with $\mathbb{K}_j^\tau$ for each $1 \le j \le Nd$, we obtain by using the orthogonality property of the $\mathbb{K}_j^\tau$'s,

$$\|\mathbb{K}_j^\tau\|_{\mathcal{H}_d}^2 \frac{\mathrm{d}y_j}{\mathrm{d}t} = \sum_{n=1}^{Nd} y_n(t)\left\langle \mathcal{A}_N\mathbb{K}_n^\tau, \mathbb{K}_j^\tau\right\rangle_{\mathcal{H}_d} + \left\langle \mathcal{F}\left(\sum_{n=1}^{Nd} y_n(t)\mathbb{K}_n^\tau\right), \mathbb{K}_j^\tau\right\rangle_{\mathcal{H}_d}. \tag{25}$$

Recall (A27), i.e., $\|\mathbb{K}_j^\tau\|_{\mathcal{H}_d} = \|\mathcal{K}_{j_q}^\tau\|_{\mathcal{H}_1}$, and recall that $\|\mathcal{K}_{j_q}^\tau\|_{\mathcal{H}_1} = \|\mathcal{K}_{j_q}\|_{\mathcal{E}}$ [see (A13)], where $\mathcal{E}$ denotes the space, $L^2([-1,1);\mathbb{R}) \times \mathbb{R}$, equipped with the inner product given by (A6).

Here and below, given an integer $1 \le j \le Nd$, the integers in $0 \le j_q \le N-1$ and $1 \le j_r \le d$ denote those obtained from the integer decomposition (A22) and (A23) and arising in the vectorization of Koornwinder polynomials; see (A24).

Due to properties of Koornwinder polynomials, the inner products in the RHS of (25) may be computed explicitly (see Appendix A 4),[54] and one obtains then the following Nd-dimensional GK approximation:

$$\frac{\mathrm{d}y_j}{\mathrm{d}t} = \frac{1}{\|\mathcal{K}_{j_q}\|_{\mathcal{E}}^2}\sum_{n=1}^{Nd}\left[\frac{2}{\tau}[P_N]_{j,n} + L_{j_r,n_r} + K_{n_q}(-1)B_{j_r,n_r} + \tau(2\delta_{n_q,0}-1)C_{j_r,n_r}\right]y_n(t)$$
$$+ \frac{1}{\|\mathcal{K}_{j_q}\|_{\mathcal{E}}^2}F_{j_r}\left(\sum_{n=1}^{Nd}y_n(t)\mathbf{K}_n(1), \sum_{n=1}^{Nd}y_n(t)\mathbf{K}_n(-1), \tau\sum_{n=1}^{Nd}(2\delta_{n_q,0}-1)\mathbf{K}_n(1)y_n(t)\right). \tag{26}$$

Here, the symbol $\delta_{j,k}$ denotes the Kronecker symbol.

The $Nd \times Nd$ matrix, P_N, results from the expansion of the derivative of a given Koornwinder polynomial in terms of the others; see (A32)–(A36) and Appendix A 2. These derivatives arise from the term $\mathcal{A}_N\mathbb{K}_n^\tau$ in (25), which involves the derivative with respect to θ, since $\mathcal{A}_N\mathbb{K}_n^\tau$ is expressed in terms of $\mathcal{A}\mathbb{K}_n^\tau$ with $\mathcal{A}$ given by (17); see (A30).

After calculations, we find [see (A36)] that the entries of P_N are given by

$$[P_N]_{j,n} = \left(\sum_{k=0}^{n_q-1} a_{n_q,k}\left(\delta_{j_q,k}\|\mathcal{K}_{j_q}\|_{\mathcal{E}}^2 - 1\right)\right)\delta_{n_r,j_r}. \tag{27}$$

The coefficients $a_{i,j}$ are obtained by solving the triangular system $\mathbf{T}\boldsymbol{a}_n = \boldsymbol{b}_n$, where the Koornwinder derivative matrix $\mathbf{T}$ and $\boldsymbol{b}_n$ is given explicitly in Proposition A.1 and depends only on n. We adopt the convention for summation that if the upper bound is less than the lower bound, the sum is set to zero.

The $L_{k,\ell}$'s, $B_{k,\ell}$'s, and $C_{k,\ell}$'s denote the entries of the $d \times d$ matrices L, B, and C in (15), respectively. See also Appendix C in Ref. 26 for further details.

The following compact form of the Nd-dimensional GK system (26) is often used hereafter:

$$\frac{\mathrm{d}\boldsymbol{y}}{\mathrm{d}t} = \Gamma_N(\tau)\boldsymbol{y} + F_N(\boldsymbol{y}), \quad \boldsymbol{y} \in \mathbb{R}^{Nd}. \tag{28}$$

Here, $\Gamma_N(\tau)\boldsymbol{y}$ denotes the linear part of Eq. (26) and $F_N(\boldsymbol{y})$ its nonlinear part. We emphasize here the explicit dependence on τ of Γ_N, keeping in mind that the dependence on the original model's linear part is contained in the coefficients of L, B, and C.

To summarize, $\Gamma_N(\tau)$ is the $Nd \times Nd$ matrix whose elements are given, for each $1 \le j \le Nd$ and $1 \le n \le Nd$, by

$$\left[\Gamma_N(\tau)\right]_{j,n} = \frac{1}{\|\mathcal{K}_{j_q}\|_{\mathcal{E}}^2}\left[\frac{2}{\tau}[P_N]_{j,n} + L_{j_r,n_r} + K_{n_q}(-1)B_{j_r,n_r} + \tau(2\delta_{n_q,0}-1)C_{j_r,n_r}\right]. \tag{29}$$

The nonlinear vector field $F_N\colon \mathbb{R}^{Nd} \to \mathbb{R}^{Nd}$ is given componentwisely by

$$\left[F_N\right]_j(\boldsymbol{y}) = \frac{1}{\|\mathcal{K}_{j_q}\|_{\mathcal{E}}^2}F_{j_r}\left(\sum_{n=1}^{Nd}y_n(t)\mathbf{K}_n(1), \sum_{n=1}^{Nd}y_n(t)\mathbf{K}_n(-1), \tau\sum_{n=1}^{Nd}(2\delta_{n_q,0}-1)\mathbf{K}_n(1)y_n(t)\right). \tag{30}$$

Here, the $\mathbf{K}_n$'s denote the (unrescaled) vectorized Koornwinder polynomials defined as in (A24) but for θ in $[-1,1]$.

With the above GK approximation U_N of U given by (23) and by using $\mathbb{K}_j^\tau = \left(\mathbf{K}_j^\tau, \mathbf{K}_j^\tau(0)\right)$ as defined in (A25), we obtain, in particular, the following approximation $\mathbf{x}_N(t)$ of $\mathbf{x}(t)$ at the current time:

$$\mathbf{x}_N(t) = \sum_{j=1}^{Nd}y_j(t)\mathbf{K}_j^\tau(0)$$
$$= \left(\sum_{n=0}^{N-1}y_{1+nd}(t), \ldots, \sum_{n=0}^{N-1}y_{d+nd}(t)\right)^{\mathrm{T}}. \tag{31}$$

Here, the second equality above follows directly from the definition of $\mathbf{K}_j^\tau$ given by (A24) together with the fact that the Koornwinder polynomials satisfy the normalization property $K_n^\tau(0) = 1$ for any n; cf. (A12).

Based on these analytic formulas, Algorithm 1 summarizes how to efficiently form a GK approximation (28) of any DDE system written under the form (15).

Algorithm 1. GK approximation: Numerical recipe

Step 1: Generate the first N Koornwinder polynomials K_n defined in (C1) and store their norms $\|\mathcal{K}_n\|_{\mathcal{E}}$ given by (A7). Generate the corresponding (unscaled) vectorized Koornwinder polynomials $\mathbf{K}_n$ given by (A24) in which $K_{j_q}^\tau(\theta)$ therein is replaced by $K_{j_q}(\theta)$ for θ in $[-1,1]$.

Step 2: For each $1 \le n \le N$, compute the coefficients $\boldsymbol{a}_n = (a_{n,0}, \ldots, a_{n,n-1})$ by solving the algebraic system $\mathbf{T}\boldsymbol{a}_n = \boldsymbol{b}_n$, with the Koornwinder derivative matrix $\mathbf{T}$ and the vector $\boldsymbol{b}_n$ given in (A18). These coefficients are needed "offline" to determine the matrix P_N given by (27).

Step 3: Form the matrix $\Gamma_N(\tau)$ by (29) and the nonlinearity F_N obtained from (30). Then, the GK approximation is thus obtained.

III. THE HOPF BIFURCATION-CHARACTERIZATION THEOREM

In this section, given a DDE system with d variables and the first N Koornwinder polynomials, we provide a characterization of Hopf bifurcations occurring in any Nd-dimensional GK system (28) for $Nd \geq 3$. Theorem III.1 shows that this characterization boils down essentially to the computation of eigenvalues and eigenvectors for the $Nd \times Nd$ matrix Γ_N and the eigenvectors for its adjoint Γ_N^* and the computation of inner products; see (38)–(40). Such a characterization is made possible by reducing the Nd-dimensional GK system into a two-dimensional normal form, which turns out to be a Stuart–Landau equation as classically encountered in the normal form theory of Hopf bifurcations;[30] see Eq. (36).

Thanks to the rigorous convergence results of Ref. 26 and Theorem III.1, it is legitimate to argue that a Hopf bifurcation, along with its type (super- or subcritical), which occurs in the DDE dynamics, is actually captured both qualitatively and quantitatively by a sufficiently high-dimensional GK approximation. This is actually supported through the application of Theorem III.1 to GK approximations of the Koren–Feingold (KF) cloud-rain model[49] in Sec. IV hereafter and of the simpler Koren, Tziperman, and Feingold (KTF) model[50] in Sec. III B.

A. The main theorem

We make the following standard assumptions on the linear and nonlinear parts of the GK system.

(H) Assume that the GK system (28) depends on a scalar parameter λ with a C^1-smooth dependence and that there exists a critical value λ_c such that a standard Hopf condition is satisfied.[36] More precisely, we assume that (i) at the critical value λ_c, the matrix Γ_N given by (29) has a pair of pure imaginary eigenvalues and all other eigenvalues have real parts less than zero and that (ii) the leading pair of eigenvalues satisfies the transversality condition $[\frac{\mathrm{d}}{\mathrm{d}\lambda}\mathrm{Re}(\beta_j(\lambda))]|_{\lambda=\lambda_c} > 0$ $(j = 1, 2)$. The latter condition writes

$$\mathrm{Re}(\beta_j(\lambda_c)) = 0, \quad \mathrm{Im}(\beta_j(\lambda_c)) \neq 0,$$
$$\left[\frac{\mathrm{d}}{\mathrm{d}\lambda}\mathrm{Re}(\beta_j(\lambda))\right]\Big|_{\lambda=\lambda_c} > 0 \quad \text{for } j = 1, 2, \tag{32}$$

and

$$\mathrm{Re}(\beta_j(\lambda_c)) < 0, \quad 3 \leq j \leq Nd. \tag{33}$$

(N) Assume that the nonlinearity F_N is of the form

$$F_N(y) = F_N^{(2)}(y, y) + F_N^{(3)}(y, y, y) + O(\|y\|^4), \tag{34}$$

where $F_N^{(2)}$ and $F_N^{(3)}$ denote the bilinear and trilinear part of F_N, respectively.

Theorem III.1: *Consider an Nd-dimensional GK system (28) approximating Eq. (15) with $Nd \geq 3$. Assume that **(H)** and **(N)** hold. Let us denote $\boldsymbol{e}_j$'s (resp. $\boldsymbol{e}_j^*$'s) the eigenvectors of the matrix Γ_N defined by (29) (resp. its adjoint Γ_N^*). Assume that there is a neighborhood $\mathcal{O}$ of λ_c, such that for each λ in $\mathcal{O}$, the matrix Γ_N is diagonal under its eigenbasis $\{\boldsymbol{e}_i \in \mathbb{C}^N : i = 1, \ldots, Nd\}$, and the eigenvalues of Γ_N satisfy the following non-resonance condition:*

$$\forall\ i_1, i_2 \in \{1, 2\},\ n \in \{3, \ldots, Nd\},\ \textit{it holds that}$$
$$\left(\langle F_N^{(2)}(\boldsymbol{e}_{i_1}, \boldsymbol{e}_{i_2}), \boldsymbol{e}_n^*\rangle \neq 0\right) \Longrightarrow \left(\beta_{i_1}(\lambda) + \beta_{i_2}(\lambda) - \beta_n(\lambda) \neq 0\right). \tag{35}$$

Then, the 2D center-manifold (CM) reduced system for the GK system (28) admits the following Stuart–Landau equation as its normal form:

$$\frac{\mathrm{d}z}{\mathrm{d}t} = \beta_1(\lambda)z + c_N(\lambda)z|z|^2 + o(|z|^3), \quad z \in \mathbb{C}, \tag{36}$$

for λ in the neighborhood $\mathcal{O}$ of λ_c.

The coefficient $c_N(\lambda)$ is given by

$$c_N(\lambda) = \left(\frac{1}{\beta_1(\lambda)} + \frac{2}{\overline{\beta}_1(\lambda)}\right) a_{20}^N a_{11}^N + \frac{1}{\beta_1(\lambda)}|a_{11}^N|^2 + \frac{2}{2\beta_1(\lambda) - \overline{\beta}_1(\lambda)}|a_{02}^N|^2 + a_{21}^N, \tag{37}$$

with

$$\begin{aligned} a_{20}^N &= \langle F_N^{(2)}(\boldsymbol{e}_1, \boldsymbol{e}_1), \boldsymbol{e}_1^*\rangle, \\ a_{02}^N &= \langle F_N^{(2)}(\boldsymbol{e}_2, \boldsymbol{e}_2), \boldsymbol{e}_1^*\rangle, \\ a_{11}^N &= \langle F_N^{(2)}(\boldsymbol{e}_1, \boldsymbol{e}_2), \boldsymbol{e}_1^*\rangle + \langle F_N^{(2)}(\boldsymbol{e}_2, \boldsymbol{e}_1), \boldsymbol{e}_1^*\rangle, \end{aligned} \tag{38}$$

and

$$\begin{aligned} a_{21}^N = {} & \langle F_N^{(3)}(\boldsymbol{e}_1, \boldsymbol{e}_1, \boldsymbol{e}_2), \boldsymbol{e}_1^*\rangle + \langle F_N^{(3)}(\boldsymbol{e}_1, \boldsymbol{e}_2, \boldsymbol{e}_1), \boldsymbol{e}_1^*\rangle + \langle F_N^{(3)}(\boldsymbol{e}_2, \boldsymbol{e}_1, \boldsymbol{e}_1), \boldsymbol{e}_1^*\rangle \\ & + \sum_{n=3}^{Nd} \frac{\langle F_N^{(2)}(\boldsymbol{e}_1, \boldsymbol{e}_2), \boldsymbol{e}_n^*\rangle + \langle F_N^{(2)}(\boldsymbol{e}_2, \boldsymbol{e}_1), \boldsymbol{e}_n^*\rangle}{2\mathrm{Re}(\beta_1(\lambda_c)) - \beta_n(\lambda_c)} \\ & \times \left[\langle F_N^{(2)}(\boldsymbol{e}_1, \boldsymbol{e}_n), \boldsymbol{e}_1^*\rangle + \langle F_N^{(2)}(\boldsymbol{e}_n, \boldsymbol{e}_1), \boldsymbol{e}_1^*\rangle\right] \\ & + \sum_{n=3}^{Nd} \frac{\langle F_N^{(2)}(\boldsymbol{e}_1, \boldsymbol{e}_1), \boldsymbol{e}_n^*\rangle}{2\beta_1(\lambda_c) - \beta_n(\lambda_c)} \left[\langle F_N^{(2)}(\boldsymbol{e}_2, \boldsymbol{e}_n), \boldsymbol{e}_1^*\rangle + \langle F_N^{(2)}(\boldsymbol{e}_n, \boldsymbol{e}_2), \boldsymbol{e}_1^*\rangle\right]. \end{aligned} \tag{39}$$

The Hopf bifurcation type is then determined by the sign of the following Lyapunov coefficient:

$$\ell_1^N(\lambda_c) = \mathrm{Re}\big(c_N(\lambda_c)\big) = \mathrm{Re}\left(\frac{a_{20}^N a_{11}^N \sqrt{-1}}{\mathrm{Im}(\beta_1(\lambda_c))} + a_{21}^N\right). \tag{40}$$

More precisely,

(i) *a subcritical Hopf bifurcation occurs if $\ell_1^N(\lambda_c) > 0$ and*
(ii) *a supercritical Hopf bifurcation occurs if $\ell_1^N(\lambda_c) < 0$.*

We refer to Appendix A 5 for a proof.

Remark III.1: *By rewriting the Stuart–Landau normal form (36) in polar coordinates, one easily derives the following expressions for the amplitude $A(\lambda)$ and the period $T(\lambda)$ of the bifurcated periodic*

solutions for λ in the vicinity of λ_c,

$$A(\lambda) \approx \sqrt{-\frac{\mathrm{Re}(\beta_1(\lambda))}{\mathrm{Re}(c_N(\lambda))}}, \text{ and}$$
$$T(\lambda) \approx \frac{2\pi}{\mathrm{Im}(\beta_1(\lambda)) - \frac{\mathrm{Re}(\beta_1(\lambda))}{\mathrm{Re}(c_N(\lambda))}\mathrm{Im}(c_N(\lambda))}. \tag{41}$$

These estimates are very useful in many applications, especially when the bifurcated limit cycle is unstable (a subcritical Hopf bifurcation) and thus difficult to determine numerically; see Sec. IV D *for an application.*

Remark III.2:

(i) *As the proof in* Appendix A 5 *indicates, the coefficients given by* (38) *and* (39) *remain the same if higher-order terms are added to the quadratic leading-order approximation of the center manifold, while F_N is still kept under its Taylor expansion* (34).

(ii) *In the particular case, $F_N(y) = F_N^{(3)}(y,y,y) + O(\|y\|^4)$ (i.e., $F_N^{(2)} = 0$), the Lyapunov coefficient derived from the center-manifold reduction using* (A54) *matches the one that would be derived from the 2D Galerkin truncation [i.e., with $\Phi = 0$ in* (A54)*]; we have $a_{20}^N = a_{02}^N = a_{11}^N = 0$; and*

$$a_{21}^N = \langle F_N^{(3)}(\boldsymbol{e}_1,\boldsymbol{e}_1,\boldsymbol{e}_2),\boldsymbol{e}_1^*\rangle + \langle F_N^{(3)}(\boldsymbol{e}_1,\boldsymbol{e}_2,\boldsymbol{e}_1),\boldsymbol{e}_1^*\rangle + \langle F_N^{(3)}(\boldsymbol{e}_2,\boldsymbol{e}_1,\boldsymbol{e}_1),\boldsymbol{e}_1^*\rangle. \tag{42}$$

This is because in this case, the leading-order approximation of the center manifold is already cubic, and it only contributes to terms of order five or higher order in Eq. (A54).

(iii) *Theorem III.1 assumes implicitly that the steady state that loses stability is the trivial one. In practice, this theorem is applied to the original system when rewritten in the perturbed variable about the (non-trivial) steady state losing its stability according to* ***(H)****; see Secs.* III B *and* IV *for examples.*

(iv) *Note that if $Nd = 2$, Theorem III.1 still applies with a_{21}^N reduced to the sum of the three first terms in the RHS of* (39).

Based on Theorem III.1, we describe the practical steps to follow in order to determine the Lyapunov coefficient, as summarized in Algorithm 2.

Thus, numerically, the only efforts are reduced to the resolution of algebraic systems with triangular matrices (i.e., to solve $\mathbf{T}\boldsymbol{a}_n = \boldsymbol{b}_n$) and the computation of spectral elements and inner products. Note that the coefficient $c_N(\lambda)$ of the Stuart–Landau equation (36) is also determined from the same ingredients.

B. Application to the KTF model

In this section, we use the KTF model (1) to illustrate in the relatively simple context of scalar DDEs the Hopf bifurcation-characterization theorem (Theorem III.1) based on the GK approximations introduced in Sec. II C. Since the proof of Theorem III.1 relies crucially on the center-manifold reduction (cf. Appendix A 5), we will also illustrate the performance of the associated 2D reduced system obtained from this reduction.

To simplify the presentation, we focus exclusively on the case $a = -1$, $b = \frac{1}{\mu}$ with $\mu = 0.29$, following Ref. 50, in which the delay parameter τ is the bifurcation parameter. Recall that the unknown h in the KTF model (1) represents the (normalized) cloud height. It admits thus only one physically relevant steady state obtained by solving $1 - h_\mu - \frac{1}{\mu}h_\mu^2 = 0$ with $h_\mu > 0$. It is given by

$$h_\mu = \frac{-\mu + \sqrt{\mu^2 + 4\mu}}{2}. \tag{43}$$

The KTF model (1) rewritten for the perturbed variable, $h_p = h - h_\mu$, is given by

$$\frac{\mathrm{d}h_p}{\mathrm{d}t} = -h_p(t) - \frac{2}{\mu}h_\mu\, h_p(t-\tau) - \frac{1}{\mu}h_p^2(t-\tau). \tag{44}$$

This DDE fits into the format of (15) in which the matrices L, B, and C therein reduce to scalars: $L = -1$, $B = -\frac{2}{\mu}h_\mu$, and $C = 0$. The nonlinearity is $F(X) = -\frac{1}{\mu}X^2$ whose argument depends only on the delayed state, i.e., $X = h_p(t-\tau)$. The GK approximations for (44) are thus of the form (28) with $d = 1$. The linear and nonlinear parts given, respectively, by (29) and (30) can be further simplified by noting that for scalar DDEs, i.e., $d = 1$, the integer pair (j_q, j_r) defined in (A22) and (A23) for any j is always given by $(j-1, 1)$. The resulting GK approximation for (44) takes thus the form

$$\frac{\mathrm{d}\boldsymbol{y}}{\mathrm{d}t} = \Gamma_N(\tau)\boldsymbol{y} + F_N(\boldsymbol{y}), \quad \boldsymbol{y} \in \mathbb{R}^N, \tag{45}$$

where the linear part is given for each $1 \le j \le N$ and $1 \le n \le N$ by

$$\left[\Gamma_N(\tau)\right]_{j,n} = \frac{1}{\|\mathcal{K}_{j-1}\|_{\mathcal{E}}^2}\left[I_{n,j}(\tau) - 1 - \frac{2}{\mu}K_{n-1}(-1)h_\mu\right], \tag{46}$$

Algorithm 2. Lyapunov coefficient $\ell_1^N(\lambda_c)$: Numerical recipe

Step 1: Compute the coefficients $\boldsymbol{a}_n = (a_{n,0}, \ldots, a_{n,n-1})$ by solving the algebraic system $\mathbf{T}\boldsymbol{a}_n = \boldsymbol{b}_n$, with the Koornwinder derivative matrix $\mathbf{T}$ and the vector $\boldsymbol{b}_n$ given in (A18). Form the matrix P_N given by (27).
Step 2: Form $\Gamma_N(\tau)$ given by (29) and compute its eigenvalues β_j and eigenvectors $\boldsymbol{e}_j$, as well as the eigenvectors $\boldsymbol{e}_j^*$ of the adjoint matrix $\Gamma_N^*(\tau)$.
Step 3: Determine the critical parameter λ_c at which the rightmost pair of eigenvalues satisfies $\mathrm{Re}(\beta_j(\lambda_c)) = 0, j = 1, 2$.
Step 4: Compute a_{20}^N, a_{11}^N, and a_{21}^N according to their formula (38) and (39), respectively, and then compute the Lyapunov coefficient $\ell_1^N(\lambda_c)$ given by (40). See Appendix C2.

with

$$I_{n,j}(\tau) = \frac{2}{\tau}\sum_{k=0}^{n-2} a_{n-1,k}\left(\delta_{j-1,k}\|\mathcal{K}_{j-1}\|_{\mathcal{E}}^2 - 1\right). \tag{47}$$

Here, the sum in the RHS of (46) is obtained from P_N given by (27), in this scalar case.

The nonlinear term, $F_N\colon \mathbb{R}^N \to \mathbb{R}^N$, is given component-wisely [see (30)] by

$$\begin{aligned}\left[F_N\right]_j(\boldsymbol{y}) &= \frac{1}{\|\mathcal{K}_{j-1}\|_{\mathcal{E}}^2} F\left(\sum_{n=1}^{N} y_n(t)K_{n-1}(-1)\right)\\ &= -\frac{1}{\mu\|\mathcal{K}_{j-1}\|_{\mathcal{E}}^2}\left(\sum_{n=1}^{N} y_n(t)K_{n-1}(-1)\right)^2,\end{aligned} \tag{48}$$

since in the scalar case ($d = 1$), $\mathbf{K}_n(\theta) = K_{n-1}(\theta)$; cf. (A24). The evaluation of the $K_{n-1}(-1)$'s is achieved through (C2), while the norms $\|\mathcal{K}_{j-1}\|_{\mathcal{E}}$ are explicitly given in (A13).

Given the GK approximation (45) thus built for a given reduced dimension N, the associated Lyapunov coefficient $\ell_1^N(\tau_c)$ defined by (40) is then computed once the critical τ_c is found; that is, the eigenelements $\{(\beta_j, \boldsymbol{e}_j) : j = 1, \ldots, N\}$ of $\Gamma_N(\tau_c)$ as well as the eigenvectors $\{\boldsymbol{e}_j^* : j = 1, \ldots, N\}$ for $\Gamma_N^*(\tau_c)$ are computed for $\tau = \tau_c$; see Algorithm 2. Note that for the computation of the Lyapunov coefficient, it is the formula (C9), similar to (48) but allowing for different arguments, that is used for the $F_N^{(2)}$-term in (40). The cubic term $F_N^{(3)}$ therein is simply zero since F_N given by (48) is quadratic.

We compute the Lyapunov coefficient $\ell_1^N(\tau_c)$ for $a = -1$, $b = \frac{1}{\mu}$ with $\mu = 0.29$. The stability analysis of Ref. 50 predicts that the critical delay parameter at which the critical equilibrium h_μ loses its stability is $\tau_c \approx 0.724$. This loss of stability is characterized by the dominant eigenpair of $\Gamma_N(\tau)$ that crosses the imaginary axis as τ crosses τ_c from below. In particular, assumption **(H)** of Sec. III A is satisfied with $\lambda_c = \tau_c$. As shown in Fig. 2, the Lyapunov coefficient is negative for all $N \geq 3$ and converges quickly as N increases. Theorem III.1 implies thus that a *supercritical Hopf bifurcation* takes thus place for any high-dimensional GK approximations of the KTF model (1).

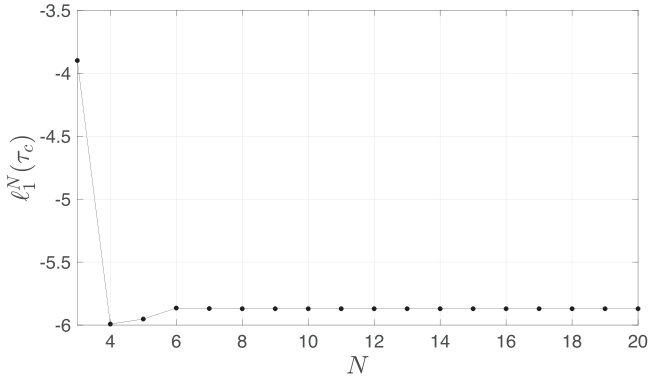

FIG. 2. The Lyapunov coefficient $\ell_1^N(\tau_c)$ (40) for the N-dimensional GK system (45) as N increases. The coefficients a_{20}^N, a_{11}^N, and a_{21}^N are computed according to their formulas (38) and (39), with the $F_N^{(2)}$-term therein given by (C9) and $F_N^{(3)}$ being identically zero. The spectral elements involved in the computations of these coefficients are those of the matrix $\Gamma_N(\tau)$ given by (46) with $\tau = \tau_c$.

C. Center-manifold reduction

Theorem III.1 predicts that near τ_c, the Stuart–Landau equation (36) provides a low-dimensional dynamical (topological) surrogate of any high-dimensional GK approximation of the KTF model and thus of the KTF dynamics itself. In our numerical calculations below, this Stuart–Landau equation is obtained from a 10D GK approximation.[55] As shown below, the combination of the GK method with center-manifold techniques allows us to extract reduced coordinates that contain most of the KF's solution energy, near criticality.

Recall that the Stuart–Landau equation (36) results from the normal form reduction of the center-manifold (CM) reduced equation, when only the leading-order terms are retained. At the core of this calculation is thus the leading-order approximation Φ_2 of the center manifold, following Theorem 2 in Ref. 37; we refer to Sec. 2 in Ref. 37 for an introduction to center-manifold reduction techniques. We describe hereafter how the CM reduced equation is derived based on GK approximations of the KTF model.

To do so, first, the GK system (45) is written under the eigenbasis $\{\boldsymbol{e}_j\}_{j=1}^N$ of Γ_N, namely,

$$\frac{\mathrm{d}z_j}{\mathrm{d}t} = \beta_j(\tau)z_j + \left\langle F_N\left(\sum_{k=1}^{N} z_k\boldsymbol{e}_k\right), \boldsymbol{e}_j^*\right\rangle, \quad j = 1, \ldots, N, \tag{49}$$

where $z_j = \langle \boldsymbol{y}, \boldsymbol{e}_j^*\rangle$ with $\boldsymbol{y}$ solving Eq. (45); here $\langle\cdot,\cdot\rangle$ denotes the inner product of $\mathbb{C}^N$ and the $\beta_i(\tau)$'s denote the eigenvalues of Γ_N.

Then, according to Eqs. (2.47) and (2.48) in Ref. 37 with $k = 2$, the CM leading-order approximation, Φ_2, is given by

$$\Phi_2(\xi) = \sum_{n=3}^{N} \Phi_{2,n}(\xi)\boldsymbol{e}_n, \quad \xi = (\xi_1, \xi_2) \in \mathbb{C}^2, \tag{50}$$

where $\Phi_{2,n}(\xi)$ is a homogeneous quadratic polynomial in the variables ξ_1 and ξ_2 given by

$$\begin{aligned}\Phi_{2,n}(\xi) = &\frac{\langle F_N^{(2)}(\boldsymbol{e}_1, \boldsymbol{e}_1), \boldsymbol{e}_n^*\rangle}{2\beta_1(\tau) - \beta_n(\tau)}(\xi_1)^2\\ &+ \frac{\langle F_N^{(2)}(\boldsymbol{e}_1, \boldsymbol{e}_2), \boldsymbol{e}_n^*\rangle + \langle F_N^{(2)}(\boldsymbol{e}_2, \boldsymbol{e}_1), \boldsymbol{e}_n^*\rangle}{2\mathrm{Re}(\beta_1(\tau)) - \beta_n(\tau)}\xi_1\xi_2\\ &+ \frac{\langle F_N^{(2)}(\boldsymbol{e}_2, \boldsymbol{e}_2), \boldsymbol{e}_n^*\rangle}{2\overline{\beta_1}(\tau) - \beta_n(\tau)}(\xi_2)^2,\end{aligned} \tag{51}$$

with $F_N^{(2)}$ given by (C9).

Using Φ_2 given by (50) and (51), the 2D CM reduced system becomes

$$\frac{\mathrm{d}z}{\mathrm{d}t} = \beta_1(\tau)z + \left\langle F_N^{(2)}\left(z\boldsymbol{e}_1 + \bar{z}\boldsymbol{e}_2 + \Phi_2(z, \bar{z})\right), \boldsymbol{e}_1^*\right\rangle, \tag{52}$$

in which we have used that $\beta_2(\tau) = \overline{\beta_1}(\tau)$ and $\boldsymbol{e}_2 = \overline{\boldsymbol{e}_1}$, due to assumption **(H)**; see (A53). Here, the variable $z(t)$ [resp. $\bar{z}(t)$]

approximates $z_1(t)$ [resp. $z_2(t)$]. Once (52) is made explicit, the Stuart–Landau equation (36) is then obtained as the normal form of Eq. (52), using standard techniques.[56]

Figure 3 shows that the CM reduced equation (52) is actually able to reproduce the KTF's embedded attractor to a very good level of accuracy for a range of τ-values above τ_c (i.e., when a stable limit cycle has emerged), although its performance is gradually downgraded[57] when τ is further increased as expected from the CM theory. Indeed, the latter theory is guaranteed to operate locally, near the critical equilibrium, whereas the periodic solution's amplitude grows as τ increases. At the same time, the nonlinear CM reduction is crucial to obtain good results of approximations near τ_c as a comparison with a 2D crude approximation reveals. Here, by crude approximation, we mean that system (49) is projected onto the dominant pair of eigenmodes of Γ_N, which consists of setting Φ_2 to zero in (52). This 2D crude truncation produces significantly less good results, predicting, in particular, unphysical negative values for $\tau \geq 0.75$. This is particularly striking as, for each τ-value used for Fig. 3, the two first eigenmodes capture more than 99% of the total energy contained in the periodic solution; see (57) for the calculation of this energy fraction.

To better appreciate this observation, recall that the CM theory predicts that for the bifurcation parameter, τ, placed sufficiently close to its critical value, τ_c, it holds that

$$\Phi_2(z_1(t), z_2(t)) \approx \sum_{n=3}^{N} z_n(t)\boldsymbol{e}_n. \tag{53}$$

The failure of the 2D crude approximation in reproducing the correct dynamics (see blue curves in Fig. 3) emphasizes thus the importance of resolving accurately the (very) small-energy contained in the term, $\sum_{n=3}^{N} z_n(t)\boldsymbol{e}_n$, in order to approximate accurately the stable limit cycle to (49). The ability of Φ_2 in approximating such small-energy terms is dealt with in Ref. 37, for general ODE systems.

The Φ_2-approximation to the center manifold is also relevant to the KTF model itself. We provide below geometric insights in that respect. To do so, we proceed as follows. First, we take the stable limit cycle, $X(t)$, to the KTF model reformulated as Eq. (44) and

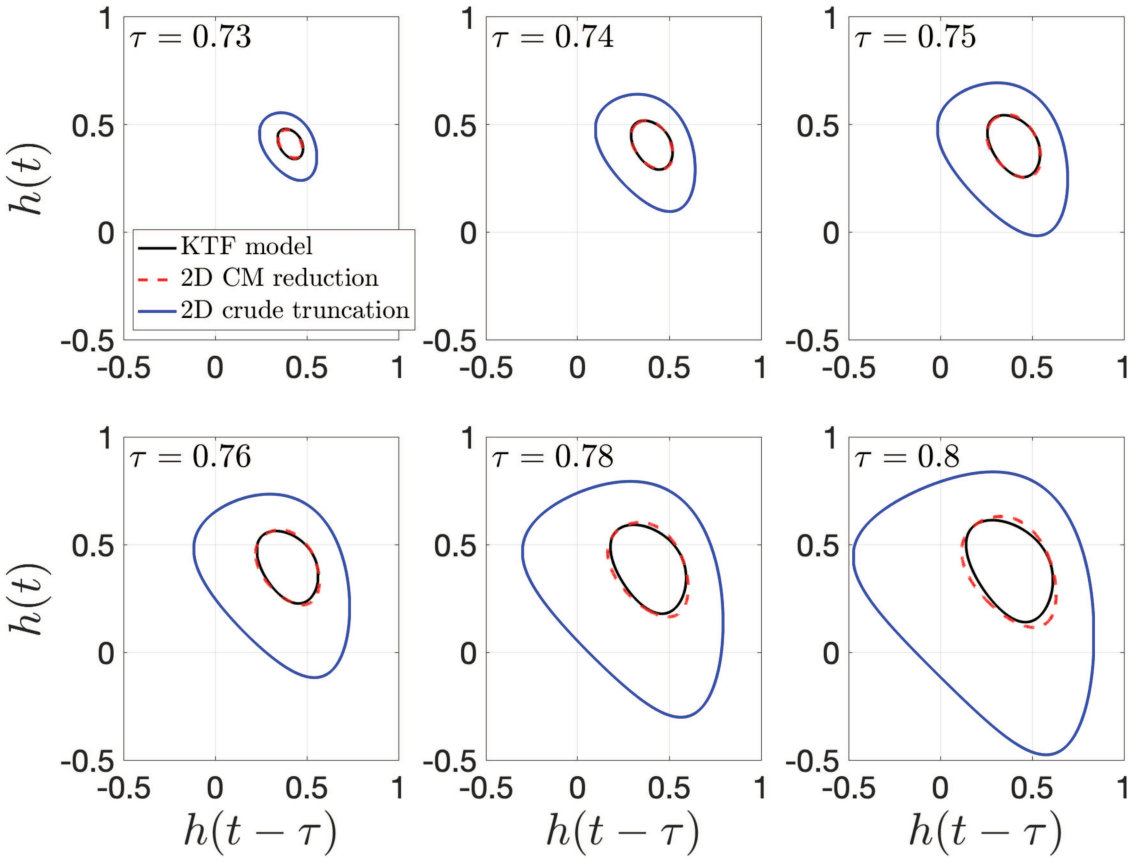

FIG. 3. Embedded attractors and ODE approximations as τ varies away from τ_c. The embedded attractors are shown within the $[h(t-\tau), h(t)]$-plane in black for the original KTF model (1) and with red dashed lines for 2D center-manifold (CM) reduction (52) as obtained from the 10D GK approximation (50) with $N = 10$. Also shown in blue is the approximation from the 2D crude truncation obtained by setting Φ_2 in (52) to zero.

project $X(t)$ onto the first N (rescaled) Koornwinder polynomials to obtain a vector $\boldsymbol{x}_N(t) = (x_1(t), \ldots, x_N(t))$ in $\mathbb{R}^N$. Recall that $X(t)$ is approximated by summing the components of $\boldsymbol{x}_N(t)$ [see (10)], such that if N is sufficiently large,

$$X(t) \approx \sum_{j=1}^{N} x_j(t). \tag{54}$$

By writing the vector $\boldsymbol{x}_N(t)$ in terms of the basis $\{\boldsymbol{e}_j\}$, we have

$$\boldsymbol{x}_N(t) = \sum_{n=1}^{N} w_n(t)\boldsymbol{e}_n, \tag{55}$$

where $w_n(t) = \langle \boldsymbol{x}(t), \boldsymbol{e}_n^* \rangle$, and we arrive, by summing over the components, at

$$\begin{aligned} X(t) &\approx \sum_{k=1}^{N}\sum_{n=1}^{N} w_n(t)\boldsymbol{e}_n^k \\ &= \underbrace{\sum_{k=1}^{N}\sum_{n=1}^{2} w_n(t)\boldsymbol{e}_n^k}_{a(t)} + \underbrace{\sum_{k=1}^{N}\sum_{n=3}^{N} w_n(t)\boldsymbol{e}_n^k}_{\epsilon(t)}, \end{aligned} \tag{56}$$

for N sufficiently large. Here, $\boldsymbol{e}_n^k$ denotes the kth component of $\boldsymbol{e}_n$.

In (56), the term $a(t)$ captures most of the energy contained in $X(t)$ ($\approx$99%), while the $\epsilon(t)$-term contains the remaining of it. Here, the percentage of energy captured by $a(t)$ is computed by using the formula

$$\frac{\int_0^T \left(|w_1(t)|^2 + |w_2(t)|^2\right)\mathrm{d}t}{\sum_{n=1}^{N}\int_0^T |w_n(t)|^2\mathrm{d}t} \times 100\%, \tag{57}$$

where T denotes the KF solution period. It is this latter small-energy contribution to $X(t)$ that is captured by the Φ_2-function and which is crucial to resolve accurately to get a good low-dimensional (here 2D) approximation.

Note that the x_j's are real [since $X(t)$ and the Koornwinder polynomials are real], and the eigenvectors $\boldsymbol{e}_n$ of Γ_N come either real or in complex conjugate pairs. Thus, since $\beta_2(\tau) = \overline{\beta_1}(\tau)$ and $\boldsymbol{e}_2 = \overline{\boldsymbol{e}_1}$, the term $a(t)$ is real, and similarly, $\epsilon(t)$ is also real for each t.

Therefore, one can form the following (closed) curve in $\mathbb{R}^3$:

$$\gamma(t) = (\mathrm{Re}(w_1(t)), \mathrm{Im}(w_1(t)), \epsilon(t)). \tag{58}$$

This curve is shown in Fig. 4 for $\tau = 0.75$ (black curve). It represents the small-energy contained in the corresponding stable limit cycle, $X(t)$, to the KTF model (44).

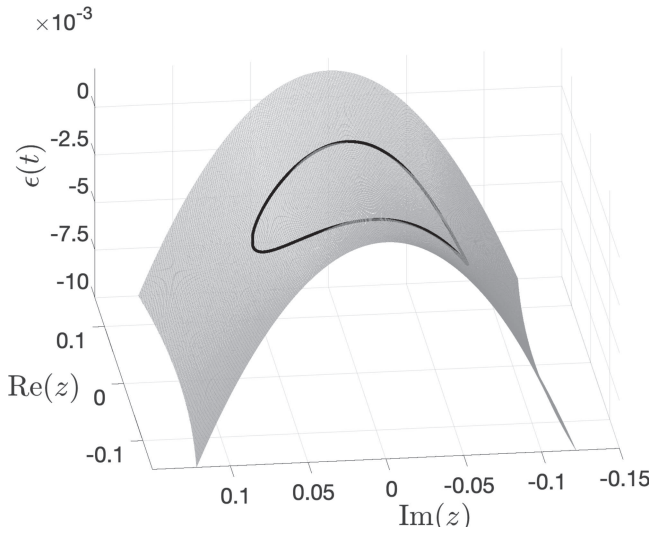

FIG. 4. Center-manifold (CM) approximation. The small-energy component $\gamma(t)$ of the KTF's stable limit cycle, $X(t)$, for $\tau = 0.75$ as given by (58) (black curve) vs the surface associated with the CM approximation Φ_2 given by (59) (gray surface).

The success in approximating $X(t)$ by the CM reduced system (52) as reported in Fig. 3 is, geometrically, characterized by the fact that the curve $\gamma(t)$ lies within a very thin neighborhood of the graph of Φ_2, after summation of the components of Φ_2. To visualize this ability of Φ_2 in approximating $\gamma(t)$, we consider the mapping

$$(\mathrm{Re}(z), \mathrm{Im}(z)) \mapsto \sum_{k=1}^{N}\sum_{n=3}^{N} \Phi_{2,n}(\xi)\boldsymbol{e}_n^k, \tag{59}$$

with $\xi = (\mathrm{Re}(z) + i\mathrm{Im}(z), \mathrm{Re}(z) - i\mathrm{Im}(z))$ and where $i^2 = -1$. The graph of this mapping is the gray surface shown in Fig. 4, for which the $\Phi_{2,n}$'s are computed according to (51) for $\tau = 0.75$.

Figure 4 shows thus the striking ability of the function Φ_2 to parameterize efficiently the small-energy term $\epsilon(t)$ as a function of $z = w_1(t)$, which shows that, near criticality, periodic solutions to the KTF model are essentially parameterized by a time-dependent complex variable, by recalling that $a(t)$ in (56) reduces to $\sum_{k=1}^{N}(w_1(t)\boldsymbol{e}_1^k + \overline{w_1}(t)\boldsymbol{e}_2^k)$. The same is true for the periodic solutions to the GK system (49) by replacing $w_1(t)$ by $z_1(t)$. Recall that $z(t)$ solving the CM reduced equation (52) approximates $z_1(t)$. Thus, if N is sufficiently large, $z_1(t)$ approximates $w_1(t)$, and we can conclude that the periodic solutions to the KTF model are well approximated by the solution $z(t)$ to Eq. (52) (with the appropriate initial data), and the DDE dynamics reduces essentially to that of a 2D ODE system (going back to real variables); see Fig. 3 again. In other words, $\mathrm{Re}(z_1)$ and $\mathrm{Im}(z_1)$ are the essential reduced coordinates that can be efficiently modeled by the reduced equation (52), for τ near its critical value τ_c. In view of generalization to the more realistic case of a network of clouds, such insights are particularly relevant and, potentially, physically useful from a modeling viewpoint.

IV. APPLICATION TO THE KOREN–FEINGOLD (KF) CLOUD-RAIN MODEL

A. GK approximation of the KF cloud-rain model

In Ref. 49, Koren and Feingold proposed the following DDE system as an elemental model for aerosol-cloud-precipitation interactions:

$$\begin{aligned}\frac{\mathrm{d}x}{\mathrm{d}t} &= \frac{b-x(t)}{s_1} - \frac{ax^2(t-\tau)}{y(t-\tau)},\\ \frac{\mathrm{d}y}{\mathrm{d}t} &= \frac{c-y(t)}{s_2} - \mathrm{d}x^3(t-\tau).\end{aligned} \tag{60}$$

The variable x characterizes the cloud depth, while y, the cloud droplet concentration. The constants s_1 and s_2 are timescales of relaxation toward the equilibrium, in the absence of coupling between x and y. The delay parameter τ accounts for lagged effects in the rain production as involving the cloud's state some period of time prior to the current time. We refer to Sec. IV D for the physical meaning of the parameters a, b, c, and d and Table I for relationships with the original formulation in Ref. 49. Note that when $d = 0$ and for t sufficiently large, system (60) reduces to the KTF model[50] analyzed in Sec. III B.

Our goal is to apply Theorem III.1 to a high-accuracy GK approximation to (60) in order to qualify the emergence of periodic oscillations as the delay parameter τ is varied. To do so, we recast system (60) in terms of fluctuation variables about the critical equilibrium that loses its stability; see Remark III.2. For this purpose, we observe that this critical equilibrium, denoted by $(\bar{x}, \bar{y})$, trivially satisfies

$$\begin{aligned}\frac{b-\bar{x}}{s_1} &= \frac{a\bar{x}^2}{\bar{y}},\\ \frac{c-\bar{y}}{s_2} &= d\bar{x}^3.\end{aligned} \tag{61}$$

Note that $(\bar{x}, \bar{y})$ does not depend on the delay parameter τ, but its linear stability does. By manipulating (61), the unknown $\bar{y}$ is eliminated, and we arrive at the following equation satisfied by $\bar{x}$:

$$ds_2\bar{x}^4 - bds_2\bar{x}^3 - as_1\bar{x}^2 - c\bar{x} + bc = 0. \tag{62}$$

An analytical form of the steady state in terms of a, b, c, d, and s_1, s_2 is thus available. For our numerical purposes, we simply solve the system (61) by, e.g., the Newton method, with the initial guess to be either the mean value of the KF model's solution of interest or the steady state of a nearby parameter regime in the spirit of a continuation method when parameter variations are considered as for Secs. IV C and IV D. For the numerical results of Sec. IV B hereafter, the steady state is found with the initial guess to be the mean value.

Once a steady state of interest is found, we consider the fluctuation variables about this steady state, namely,

$$u = x - \bar{x}, \quad v = y - \bar{y}. \tag{63}$$

We rewrite (60) in the fluctuation variables. To do so, we assume the fluctuation v to be small, which leads to

$$\begin{aligned}\frac{1}{y(t-\tau)} &= \frac{1}{\bar{y}}\left(1 + \tfrac{v(t-\tau)}{\bar{y}}\right)^{-1}\\ &= \frac{1}{\bar{y}}\left(1 - \frac{v(t-\tau)}{\bar{y}} + \left(\frac{v(t-\tau)}{\bar{y}}\right)^2\right.\\ &\quad \left. - \left(\frac{v(t-\tau)}{\bar{y}}\right)^3\right) + o(|v|^4).\end{aligned} \tag{64}$$

Using (64), we arrive (neglecting the 4th-order and higher-order terms), after rearrangement of the terms, at the following rewriting of the KF system in the u- and v-variables,

$$\frac{\mathrm{d}}{\mathrm{d}t}\begin{pmatrix}u\\ v\end{pmatrix} = L\begin{pmatrix}u(t)\\ v(t)\end{pmatrix} + B\begin{pmatrix}u(t-\tau)\\ v(t-\tau)\end{pmatrix} + \boldsymbol{F}(u(t-\tau), v(t-\tau)), \tag{65}$$

where L and B are the 2×2 matrices given by

$$L = \begin{pmatrix}-\frac{1}{s_1} & 0\\ 0 & -\frac{1}{s_2}\end{pmatrix}, \quad B = \begin{pmatrix}-\frac{2a\bar{x}}{\bar{y}} & \frac{a\bar{x}^2}{\bar{y}^2}\\ -3d\bar{x}^2 & 0\end{pmatrix}, \tag{66}$$

and the nonlinear term $\boldsymbol{F}$ is given by

$$\boldsymbol{F} = \boldsymbol{F}^{(2)} + \boldsymbol{F}^{(3)}, \tag{67}$$

with[58]

$$\boldsymbol{F}^{(2)}(p,q) = \begin{pmatrix}-\frac{ap^2}{\bar{y}} + \frac{2a\bar{x}pq}{\bar{y}^2} - \frac{a\bar{x}^2q^2}{\bar{y}^3}\\ -3d\bar{x}p^2\end{pmatrix} \tag{68}$$

and

$$\boldsymbol{F}^{(3)}(p,q) = \begin{pmatrix}\frac{ap^2q}{\bar{y}^2} - \frac{2a\bar{x}pq^2}{\bar{y}^3} + \frac{a\bar{x}^2q^3}{\bar{y}^4}\\ -dp^3\end{pmatrix}. \tag{69}$$

To determine the GK approximation of system (65), we first calculate the approximation $\boldsymbol{F}_N$ of the nonlinear term, $\boldsymbol{F}$, by using the general formula (30) that we specify to this particular example. First, observe that the integer pairs (j_q, j_r) and (n_q, n_r) appearing in (30) related to j and n, respectively, according to (A22) and (A23)

TABLE I. Notations used in Ref. 49 compared to those of the KF model (60).

Notations in (60)	x	y	a	b	c	d	s_1	s_2	τ
Notations in Ref. 49	H	N_d	α/c_1	H_0	N_0	αc_2	τ_1	τ_2	T'
Units	m	cm^{-3}	$\mathrm{cm}^{-3}\,\mathrm{m}^{-1}\,\mathrm{min}^{-1}$	m	cm^{-3}	$\mathrm{cm}^{-3}\,\mathrm{m}^{-3}\,\mathrm{min}^{-1}$	min	min	min

take here the following simple form (because $d = 2$):

$$(n_q, n_r) = \begin{cases} \left(\frac{n-1}{2}, 1\right) & \text{if } n \text{ is odd,} \\ \left(\frac{n-2}{2}, 2\right) & \text{if } n \text{ is even,} \end{cases} \tag{70}$$

with the same identities for (j_q, j_r).

Thus, the vectorized Koornwinder polynomial $\mathbf{K}_n$ given by (A24) (before rescaling) becomes

$$\mathbf{K}_n(\theta) = \begin{cases} (K_{(n-1)/2}(\theta), 0)^{\mathrm{T}} & \text{if } n \text{ is odd,} \\ (0, K_{(n-2)/2}(\theta))^{\mathrm{T}} & \text{if } n \text{ is even.} \end{cases} \tag{71}$$

Here, K_p denotes the pth Koornwinder polynomial (defined over $[-1,1]$); see Appendix A 1.

Next, note that the term $\sum_{n=1}^{2N} y_n(t)\mathbf{K}_n(-1)$ in (30) is aimed at approximating $(u(t-\tau), v(t-\tau))$. Componentwise, it means that the lagged variables, $u_N(t-\tau)$ and $v_N(t-\tau)$, are given by

$$u_N(t-\tau) = \sum_{n=1}^{N} y_{2n-1}(t) K_{n-1}(-1),$$
$$v_N(t-\tau) = \sum_{n=1}^{N} y_{2n}(t) K_{n-1}(-1) \tag{72}$$

[with $\boldsymbol{y}(t)$ solving (28)] approximate $u(t-\tau)$ and $v(t-\tau)$, respectively; see (23). Recall that the $K_{n-1}(-1)$'s are given by (C2).

The sought nonlinear term $\boldsymbol{F}_N$ is decomposed into $\boldsymbol{F}_N = \boldsymbol{F}_N^{(2)} + \boldsymbol{F}_N^{(3)}$ by grouping quadratic and cubic terms. Given any $\boldsymbol{y}$ in $\mathbb{R}^{2N}$, let us denote

$$p = \sum_{n=1}^{N} y_{2n-1} K_{n-1}(-1),$$
$$q = \sum_{n=1}^{N} y_{2n} K_{n-1}(-1). \tag{73}$$

Thus, finally, the general formula (30) takes the following form in which $\boldsymbol{F}_N^{(2)}$ and $\boldsymbol{F}_N^{(3)}$ approximate $\boldsymbol{F}^{(2)}$ and $\boldsymbol{F}^{(3)}$ given by (68) and (69), respectively:

$$\left[F_N^{(2)}\right]_j(\boldsymbol{y}, \boldsymbol{y}) = \begin{cases} \dfrac{\boldsymbol{F}_1^{(2)}(p,q)}{\|\mathcal{K}_{(j-1)/2}\|_{\mathcal{E}}^2} = \dfrac{1}{\|\mathcal{K}_{(j-1)/2}\|_{\mathcal{E}}^2}\left(-\dfrac{ap^2}{\bar{y}} + \dfrac{2a\bar{x}pq}{\bar{y}^2} - \dfrac{a\bar{x}^2q^2}{\bar{y}^3}\right) & \text{for } j \text{ is odd,} \\ \dfrac{\boldsymbol{F}_2^{(2)}(p,q)}{\|\mathcal{K}_{(j-2)/2}\|_{\mathcal{E}}^2} = -\dfrac{3d\bar{x}p^2}{\|\mathcal{K}_{(j-2)/2}\|_{\mathcal{E}}^2} & \text{for } j \text{ is even,} \end{cases}$$
$$\left[F_N^{(3)}\right]_j(\boldsymbol{y}, \boldsymbol{y}, \boldsymbol{y}) = \begin{cases} \dfrac{\boldsymbol{F}_1^{(3)}(p,q)}{\|\mathcal{K}_{(j-1)/2}\|_{\mathcal{E}}^2} = \dfrac{1}{\|\mathcal{K}_{(j-1)/2}\|_{\mathcal{E}}^2}\left(\dfrac{ap^2q}{\bar{y}^2} - \dfrac{2a\bar{x}pq^2}{\bar{y}^3} + \dfrac{a\bar{x}^2q^3}{\bar{y}^4}\right) & \text{for } j \text{ is odd,} \\ \dfrac{\boldsymbol{F}_2^{(3)}(p,q)}{\|\mathcal{K}_{(j-2)/2}\|_{\mathcal{E}}^2} = -\dfrac{dp^3}{\|\mathcal{K}_{(j-2)/2}\|_{\mathcal{E}}^2} & \text{for } j \text{ is even.} \end{cases} \tag{74}$$

In (74), the terms $\boldsymbol{F}_1^{(2)}$ (resp. $\boldsymbol{F}_2^{(2)}$) denote the first (resp. second) component of $\boldsymbol{F}^{(2)}$, with the same convention for $\boldsymbol{F}^{(3)}$.

The $2N$-dimensional GK approximation of (65) is then given by

$$\frac{\mathrm{d}\boldsymbol{y}}{\mathrm{d}t} = \Gamma_N(\tau)\boldsymbol{y} + \boldsymbol{F}_N^{(2)}(\boldsymbol{y}, \boldsymbol{y}) + \boldsymbol{F}_N^{(3)}(\boldsymbol{y}, \boldsymbol{y}, \boldsymbol{y}), \tag{75}$$

with $\Gamma_N(\tau)$ being the $2N \times 2N$ matrix whose entries in (29) take the following form:

$$\left[\Gamma_N(\tau)\right]_{j,n} = \frac{1}{\|\mathcal{K}_{j_q}\|_{\mathcal{E}}^2}\left[\frac{2}{\tau}[P_N]_{j,n} + L_{j_r,n_r} + K_{n_q}(-1)B_{j_r,n_r}\right], \tag{76}$$

since there are no distributed delay terms in the linear part of (65) [i.e., $C = 0$ in (29)]. Note that here, the integer pairs (j_q, j_r) and (n_q, n_r) satisfy the simple relation (70). Note also that for the computation of the Lyapunov coefficient, it is the formulas (B4) and (B5), similar to (74) but allowing for different arguments, that are used for the $\boldsymbol{F}_N^{(2)}$- and $\boldsymbol{F}_N^{(3)}$-terms in (40).

We recall that, once $\boldsymbol{y}(t)$ is obtained by integrating Eq. (75), an approximation $(u_N(t), v_N(t))$ of $(u(t), v(t))$ is obtained according to (31), which takes here the simple form

$$(u_N(t), v_N(t)) = \left(\sum_{n=1}^{N} y_{2n-1}(t), \sum_{n=1}^{N} y_{2n}(t)\right)^{\mathrm{T}}. \tag{77}$$

B. Characterization of Hopf bifurcations: First numerical results

We thus apply the GK method to the KF model; see Algorithm 1. For $N = 5$, i.e., corresponding here to a 10D GK system (75), we already obtained a very good approximation of the KF model's solutions, when the latter settles down to a stable periodic orbit; see Fig. 5. The numerical results are obtained for the following parameter values:

$$a = 1.5,\ b = c = d = 1,$$
$$s_1 = 10,\ s_2 = 14,\ \text{and } \tau = 2.5. \tag{78}$$

Throughout this section, the numerical solutions to the KF model are obtained by using the DDE solver as described in Appendix C 3.

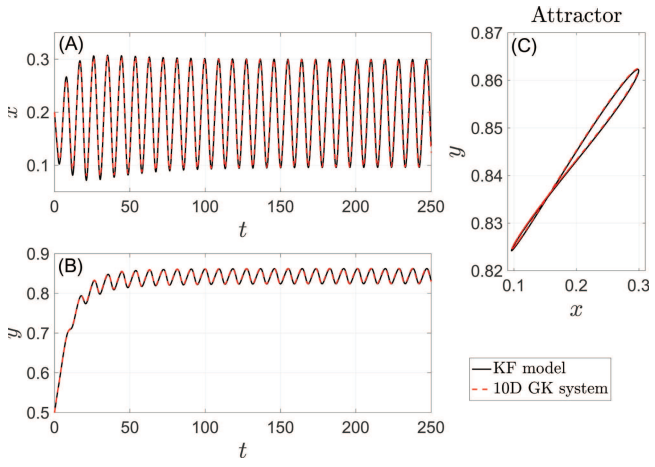

FIG. 5. Approximation skills of the 10D GK system (75). Panels (a) and (b): The solution $(x(t), y(t))$ to the (full) KF model (60) is shown in black and the one obtained by solving the 10D GK system (75) in red. More precisely, $\overline{x} + u_N(t)$ (resp, $\overline{y} + v_N(t)$) approximating $x(t)$ [resp. $y(t)$] obtained from (77) is shown in red. Panel (c): The attractor in the xy-plane. These results are obtained for the parameters listed in (78).

Using this solver to provide a reference solution, our 10D GK approximation leads to a relative error of about 3×10^{-2}% (measured in L^2-norm) when compared to the KF model's limit cycle.

The selection of the reduced dimension N is guided by the analysis of the eigenvalue problem associated with the linearization of the KF model at the steady state $(\overline{x}, \overline{y})$, i.e., the spectrum associated with the linear DDE,

$$\dot{X} = LX + BX(t-\tau), \quad X \in \mathbb{R}^2, \tag{79}$$

with L and B given in (66). For a useful set of results regarding the stability analysis of such a linear delay system, we refer to Chaps. 3.6 and 3.7 in Ref. 59.

At the core of the stability analysis to Eq. (79) is the characteristic equation. The latter is obtained by substitution of a sample solution of the form $e^{\beta t}v$, with v in $\mathbb{C}^2\backslash\{0\}$, that leads to the following characteristic equation:

$$\det \Delta(\beta, \tau) = 0, \tag{80}$$

where

$$\Delta(\beta, \tau) = \beta I_2 - L - Be^{-\beta\tau} \tag{81}$$

is the characteristic matrix.

We have found that for the parameter regime (78), the dominant pair of eigenvalues of Γ_N given in (76) approximates well the dominant eigenpair from the KF model, for $N = 5$; thus, the 10D GK approximation is used; see the left panel of Fig. 6. Here, we have used the DDE-BIFTOOL Matlab package[21] to compute the eigenvalues of the KF model's linearization, which are checked here to satisfy the characteristic equation (80) with an error smaller than 4.5×10^{-11} for each of the 40 eigenvalues shown by black circles in Figs. 6 and 7, while the dominant eigenvalues satisfy Eq. (80) to machine precision.

The left panel of Fig. 6 shows a very good approximation of the resulting three dominant eigenvalues by the dominant eigenvalues of Γ_N, while other spurious eigenvalues are produced by Γ_N. These spurious eigenvalues are further pushed away toward high frequencies as N increases [i.e. $\mathrm{Im}(\beta_j)$ getting larger as N grows] accompanied by a very good approximation of a core of eigenvalues growing with N; see Fig. 7. These numerical results about the approximation of the spectrum associated with (79) are actually consistent with the rigorous and general convergence results of $\mathcal{A}_N$ [defined in (22)] to $\mathcal{A}$ [defined in (17)] proved in Ref. 26; see Lemma 4.1 therein.

The right panel of Fig. 6 shows that the rightmost real part of the KF's linearized spectrum experiences a change of sign as τ crosses from below a critical value τ_c, while the transversality condition (32) holds; see the black curve. The same observation holds regarding the rightmost real part of the spectrum of Γ_N for the 10D GK system; see the red dashed curve in the right panel of Fig. 6. This together with the fact that conditions (33) and (35) hold here for the parameter regime considered shows that condition (**H**) of Sec. III A is satisfied. Thus, Theorem III.1 applies to this 10D GK system, and one concludes that the closed orbit shown in panel (c) of Fig. 5 arises through a Hopf bifurcation.

To qualify this Hopf bifurcation, whether it is supercritical or subcritical, we compute the Lyapunov coefficient $\ell_1^N(\lambda_c)$ according to Algorithm 2 with $\lambda_c = \tau_c \approx 2.393$ and with the $\boldsymbol{F}_N^{(2)}$- and $\boldsymbol{F}_N^{(3)}$-terms given here by (B4) and (B5), respectively. The results are shown in Fig. 8 as N increases. Without any ambiguity, the Lyapunov coefficient $\ell_1^N(\tau_c)$ converges to a negative value, showing that a supercritical Hopf bifurcation takes place (Theorem III.1) not only for $N = 5$, but also for any higher-dimensional GK approximations of the KF model.

C. Probing the parameter space: Coexistence of subcritical and supercritical Hopf bifurcations

In this section, we analyze in greater detail the type of Hopf bifurcation that occurs in the KF model. For this purpose, we investigate the parameter dependence on a and d of the Lyapunov coefficient $\ell_1^N(\tau_c)$ of a (high-dimensional) GK approximation (75) of the KF model, for which the delay parameter τ plays here also the role of the bifurcation parameter λ in Theorem III.1. More precisely, we first estimate the critical delay τ_c, at which the critical equilibrium loses its stability, and then compute the Lyapunov coefficient $\ell_1^N(\tau_c)$ for (a, d) varying in the square $\mathcal{D} = [0.5, 5] \times [0.5, 5]$, while the other parameters b, c, s_1, and s_2 are set as in (78). Since the parameters a and d control the intensity of the KF model's nonlinear effects, it is expected that their variations impact the Lyapunov coefficient $\ell_1^N(\tau_c)$ due to the dependence of the latter on the nonlinear terms, $\boldsymbol{F}_N^{(2)}$ and $\boldsymbol{F}_N^{(3)}$, through the coefficients a_{21}^N, a_{20}^N, and a_{11}^N; see (40). Recall that the $\boldsymbol{F}_N^{(2)}$- and $\boldsymbol{F}_N^{(3)}$-terms are

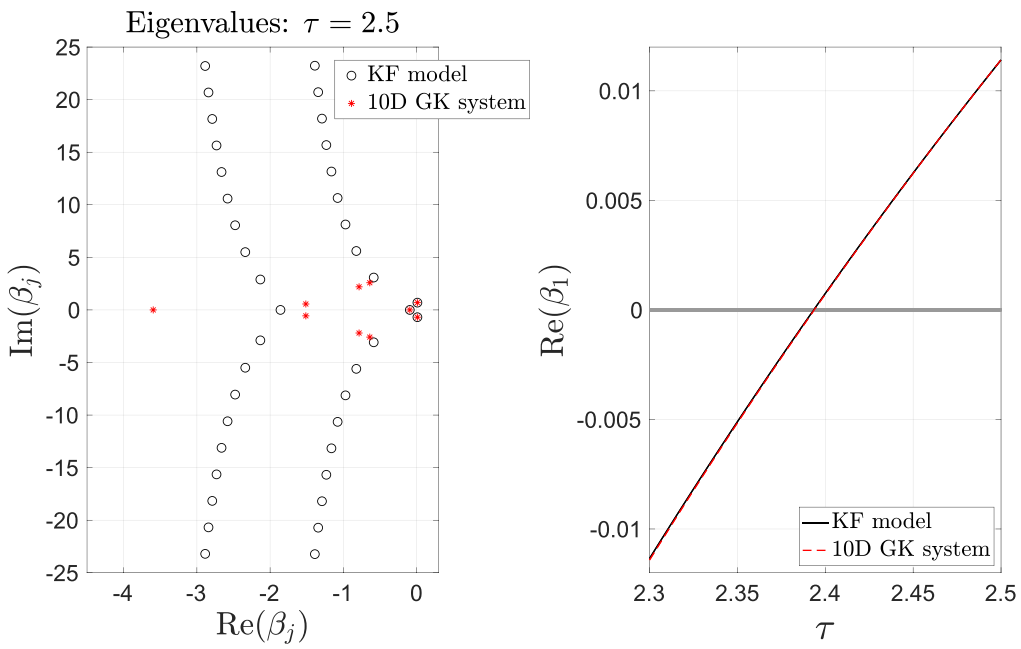

FIG. 6. Left panel: Eigenvalues obtained from the KF model linearized (black circles) at the critical equilibrium vs the eigenvalues of Γ_N given in (76) with $N = 5$ (red asterisks) and for the parameter values in (78). Here, the DDE-BIFTOOL Matlab package has been used[21] to compute the eigenvalues of the linearized KF model (79). Right panel: The real part of the rightmost eigenvalue of (79) (black curve) and of the GK system for $N = 5$ (red dashed curve). Here, τ plays the role of the bifurcation parameter λ in (32). The critical parameter value is $\tau_c \approx 2.393$.

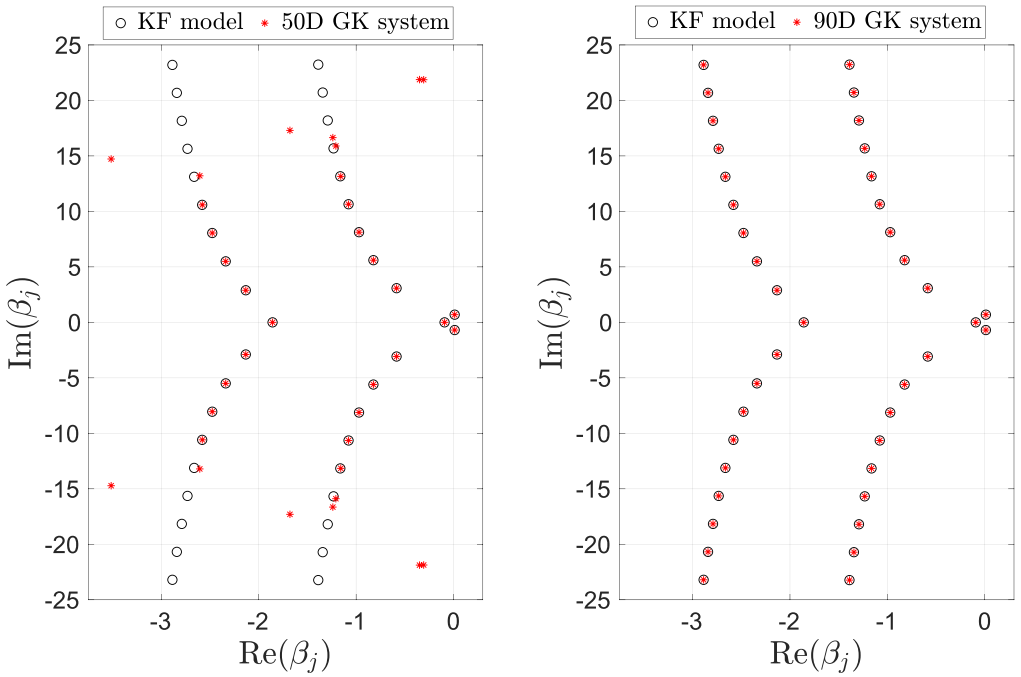

FIG. 7. Same as in the left panel of Fig. 6 except that the eigenvalues from Γ_N (red asterisks) are computed for $N = 25$ (left panel) and $N = 45$ (right panel).

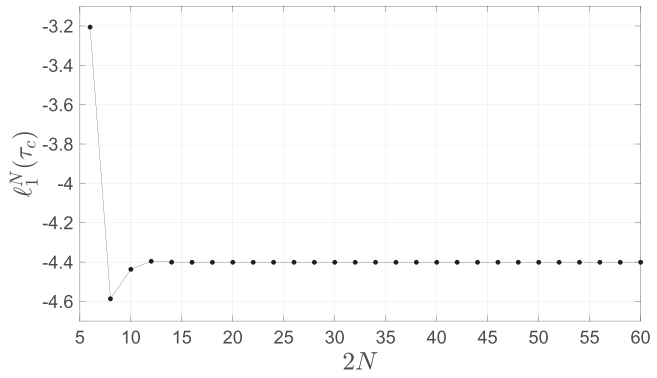

FIG. 8. The Lyapunov coefficient $\ell_1^N(\tau_c)$ (40) for the $2N$-dimensional GK system (75) as N increases. The coefficients a_{20}^N, a_{11}^N, and a_{21}^N are computed according to their formulas (38) and (39), with the $\boldsymbol{F}_N^{(2)}$- and $\boldsymbol{F}_N^{(3)}$-terms given here by (B4) and (B5), respectively. The spectral elements involved in the computations of these coefficients are those of the matrix Γ_N given by (76). The model's parameters are those used for Fig. 5 except for τ.

given here by (B4) and (B5), respectively. Note that the steady state $(\bar{x}, \bar{y})$ in these formulas is found as follows. Given a grid mesh of the domain $\mathcal{D}$ and a steady state $(\bar{x}_{p_1}, \bar{y}_{p_1})$ available at a grid point $p_1 = (a, d)$, the steady state $(\bar{x}_{p_2}, \bar{y}_{p_2})$ for a nearby grid point $p_2 = (a + \delta a, d + \delta d)$ is found by solving Eq. (62) [replacing a (resp. d) with $a + \delta a$ (resp. $d + \delta d$)] with the Newton method initiated from the initial guess $(\bar{x}_{p_1}, \bar{y}_{p_1})$. This continuation procedure for the steady state search is initiated from the grid point (a, d) corresponding to (78) (i.e., $a = 1.5$ and $d = 1$) for which the corresponding steady state is computed from Eq. (62) with the initial guess being the mean value of the KF model's solution.

The discretization of the domain $\mathcal{D}$ is organized as follows. First, the domain $\mathcal{D}$ is discretized as follows: 200 grid points along the a-direction and 1000 along the d-direction. Then, for each discrete value of d, we identify subintervals of a-values at which the Lyapunov coefficient falls within $[-1, 1]$ and perform mesh refinement of these subintervals until, e.g., a change of sign of $\ell_1^N(\tau_c)$ is resolved to a stable precision. In each of these scanning actions of the domain, the Lyapunov coefficient is computed according to Algorithm 2 for a set dimension, namely, $N = 25$ here.

The numerical results are shown in panel (b) of Fig. 9 and reveal an unambiguous coexistence of large regions of the parameter space in which subcritical and supercritical Hopf bifurcations take place. Figure 10 illustrates, for the KF model, the type of dynamical behavior associated with a subcritical Hopf bifurcation [panel (a)] and a supercritical one [panel (b)]. The parameter values are specified in the caption of this figure. We emphasize that while a stable limit cycle is always produced for $\tau > \tau_c$ according to a supercritical Hopf bifurcation, this is not always the case for a subcritical Hopf bifurcation even for $\tau < \tau_c$. It depends actually on the nonlinear dissipative effects in the neighborhood of the unstable limit cycle produced via a subcritical Hopf bifurcation. If the latter are

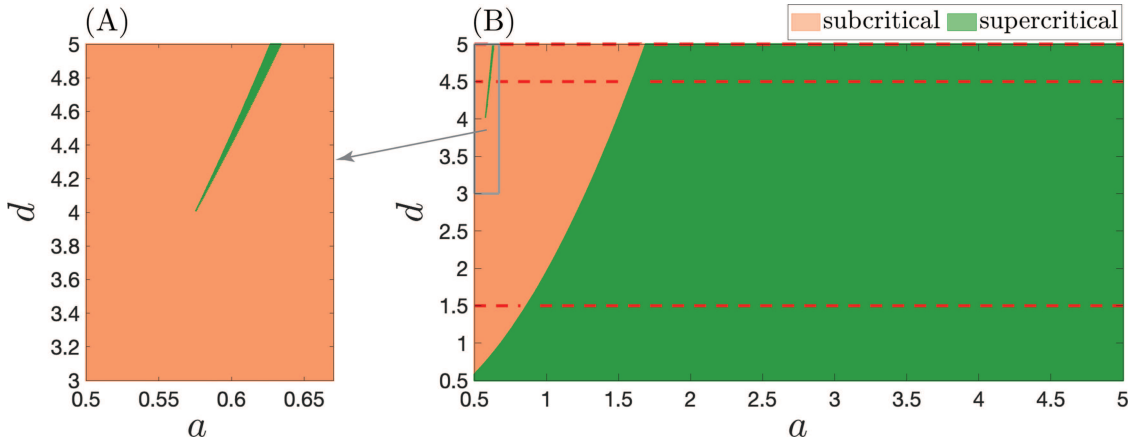

FIG. 9. Panel (a): Zoom of panel (b) for $0.5 \leq a \leq 0.67$ and $3 \leq d \leq 5$. Panel (b): Lyapunov coefficient chart. This 2D chart displays the sign of the Lyapunov coefficient $\ell_1^N(\tau_c)$ given by (40) and computed according to Algorithm 2 with $N = 25$ in the GK system (75). The parameter values are those of (78) except for a and d that are varied within $[0.5, 5]$, while τ is set to its corresponding critical value τ_c. The (a, d)-values for which a supercritical Hopf bifurcation $[\ell_1^N(\tau_c) < 0]$ takes place are shown in green, while the "salmon"-color indicates a subcritical Hopf bifurcation $[\ell_1^N(\tau_c) > 0]$. The horizontal red dashed lines indicate sections of this 2D chart along the a-direction. These sections are shown in greater detail in Fig. 11.

strong enough, then a stable limit cycle coexists somewhere nearby this unstable limit cycle, for the subcritical case. Panel (a) of Fig. 10 illustrates such a situation and shows a stable limit cycle for the subcritical case when the parameter τ is set right before its corresponding critical value, τ_c. In this case, two local attractors coexist: the critical equilibrium that is locally stable and a limit cycle also locally stable for $\tau < \tau_c$ and sufficiently close to τ_c. Two trajectories converging to these local attractors are shown in panel (a). In the supercritical case, the critical equilibrium X_{eq} when stable (for $\tau < \tau_c$) does not coexist with a limit cycle, and a stable limit cycle emerges only for $\tau > \tau_c$ while X_{eq} becomes unstable. Panel (b) of Fig. 10 shows such a situation with a trajectory converging toward the limit cycle. Note that seemingly, this trajectory goes through the unstable critical equilibrium, which is actually an artifact due to the projection onto the (x, y)-plane; the KF model's numerical trajectory is lying indeed within a much higher dimensional state space.

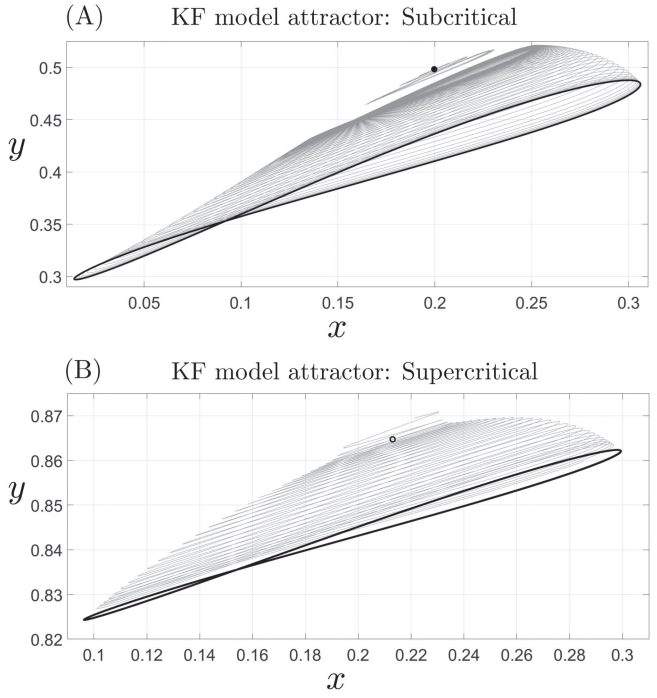

FIG. 10. Panel (a): *A subcritical case* [$\tau = 2.56$, $a = 1$, $d = 4.5$, other parameters as in (78)]. The trajectories (light gray curves) are either attracted toward the critical equilibrium (a filled circle) or the limit cycle (a thick closed curve) that emerged through a subcritical Hopf bifurcation scenario. The selection of the local attractor to which a given solution converges depends on the basin of attraction in which the initial datum falls in. Panel (b): *A supercritical case* [$\tau = 2.5$, $a = d = 1$, other parameters as in (78)]. The trajectories are attracted toward the limit cycle (a thick closed curve) that emerged through a supercritical Hopf bifurcation scenario. In this case, the critical equilibrium (an empty circle) is always a repeller. These KF model's solutions are obtained by using the DDE solver as described in Appendix C 3.

Noteworthy is also an "island" or "dike" of supercritical Hopf bifurcations within a subcritical Hopf bifurcation "sea." This dike is contained within the subdomain $[0.5, 0.65] \times [4, 5]$ of the (a, d)-plane; see panel (b) of Fig. 9. Panel (a) of Fig. 9 shows a magnified version of this region. Given our discretization, we observe, for each d in $[4, 5]$, that as the parameter a is increased from 0.5 to 0.65, the Lyapunov coefficient $\ell_1^N(\tau_c)$ becomes negative over a small interval of a-values preceding a jump discontinuity when $\ell_1^N(\tau_c)$ gets back to a positive value; see panels (d) and (e) of Fig. 11 for an illustration.

This jump discontinuity in the Lyapunov coefficient is associated with a *double-Hopf bifurcation* (codimension-two bifurcation) taking place when the linearized dynamics at the critical equilibrium exhibits two pairs of purely imaginary eigenvalues; see Fig. 12. Here again, the DDE-BIFTOOL Matlab package[21] has been used to compute the eigenvalues of the KF model's linearization with cross-checking from the characteristic equation (80). The double-Hopf bifurcations occur exactly at the parameter values at which the Lyapunov coefficient is discontinuous and are marked by the vertical dashed lines in panels (d) and (e) of Fig. 11. To this discontinuity in the Lyapunov coefficient corresponds a cusp occurring on the curve showing the dependence on the parameter a of the critical delay τ_c; see panels (a) and (b) of Fig. 11. Elsewhere, the Lyapunov coefficient depends smoothly on the parameter a, and no cusp point is observed on the corresponding τ_c-curve; see, e.g., panels (c) and (f) in Fig. 11.

D. Physical parameter regimes

We show in this section that the understanding gained from Sec. IV C based on the Hopf bifurcation Theorem III.1 allows, in particular, for providing key dynamical insights about the numerical results reported in Ref. 49. We focus on the parameter regime underlying (Fig. 6 in Ref. 49). For this purpose, we make precise in Table I the correspondence between the variables/parameters used here and those used in Ref. 49. Note that the units of the coefficients a and d given in Table I are chosen to ensure consistent physical dimensions between the nonlinear terms and the other linear and constant terms in (60). Table II provides the corresponding values of the model's coefficients for our formulation (60). These values correspond to the parameter values used for Fig. 6 in Ref. 49, taking into account the correction of the c_2-parameter in the original KF model's notations pointed out by the authors themselves; see the online version of Ref. 49.

More precisely, in the original notations of Ref. 49, $\alpha = 2\,\mathrm{mm\,m^{-6}\,d^{-1}}$, $c_1 = 2 \times 10^{-6}\,\mathrm{mm\,m^{-2}}$, $c_2 = 3 \times 10^4\,\mathrm{m^{-1}}$, $\tau_1 = \tau_2 = 60\,\mathrm{min}$, $H_0 = 530\,\mathrm{m}$, $N_0 = 180\,\mathrm{cm^{-3}}$, and $T' = 12\,\mathrm{min}$; see Table I for the parameter correspondence. Note that $\alpha/c_1 = 10^6\,\mathrm{m^{-4}\,d^{-1}} = 1/(24 \times 60)\,\mathrm{cm^{-3}\,m^{-1}\,min^{-1}}$, with the factor $1/(24 \times 60)$ arising from the conversion of $\mathrm{d^{-1}}$ to $\mathrm{min^{-1}}$. Thus, $a = 1/(24 \times 60) \approx 6.9444 \times 10^{-4}\,\mathrm{cm^{-3}\,m^{-1}\,min^{-1}}$. This conversion is to ensure the physical dimension of the nonlinear term in (60), ax^2/y, to match that of the other terms in the

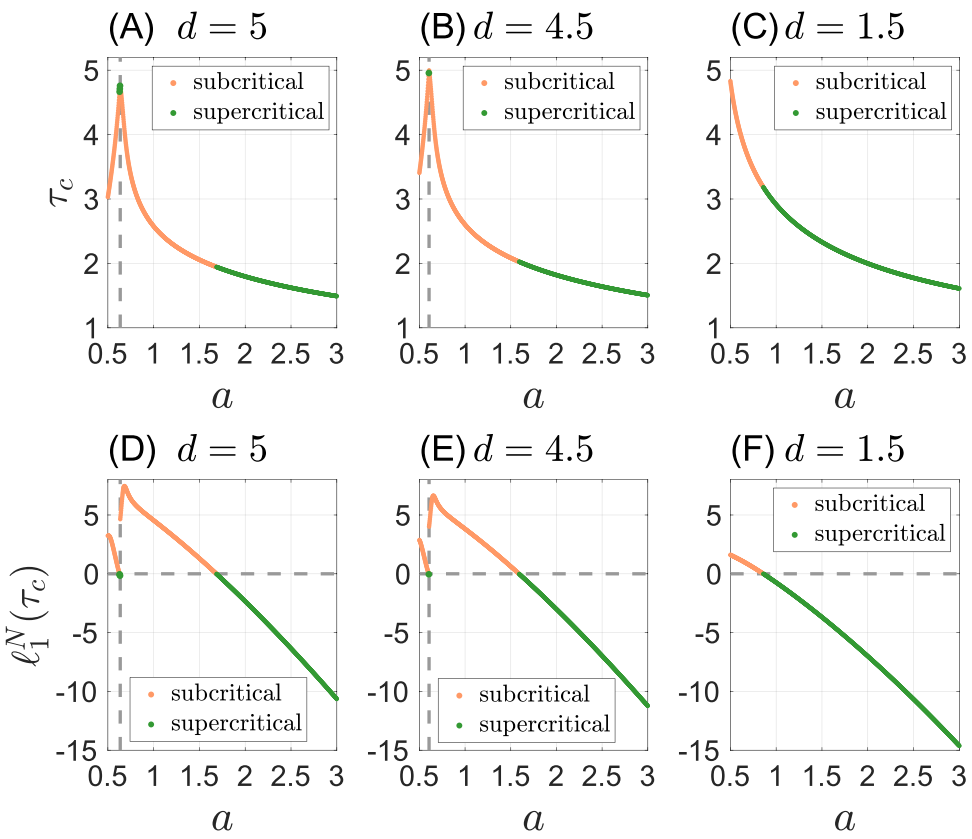

FIG. 11. Top row: Parameter dependence on a of the critical delay parameter τ_c for different values of d. Bottom row: Same but for the Lyapunov coefficient $\ell_1^N(\tau_c)$ given by (40) for $N = 25$. The latter curves correspond to the sections of the 2D Lyapunov chart shown by horizontal red dashed lines in Fig. 9. The horizontal gray dashed lines in panels (d)–(f) indicate the boundary between super- and subcritical Hopf bifurcations. The vertical gray dashed lines in panels (a), (b), (d), and (e) indicate the a-value at which a double-Hopf bifurcation occurs for the respective d-value. These critical values of the parameter a correspond to a cusp on the τ_c-curve and a jump on the $\ell_1^N(\tau_c)$-curve.

equation. For the same reason, the dimension of αc_2 is converted to $\mathrm{cm}^{-3}\,\mathrm{m}^{-3}\,\mathrm{min}^{-1}$ to obtain the numerical value of $d = 6 \times 10^{-5}/(24 \times 60) \approx 4.1667 \times 10^{-8}\,\mathrm{cm}^{-3}\,\mathrm{m}^{-3}\,\mathrm{min}^{-1}$.

Within this parameter setting, Fig. 6 of Ref. 49 was obtained for $\tau = T' = 12\,\mathrm{min}$, which turns out to correspond to a τ-value smaller than the critical value estimated here to be $\tau_c = 25.232$, explaining thus the damped oscillation observed in Fig. 6 of Ref. 49. To analyze the nature of the Hopf bifurcation associated with this critical value, we computed the Lyapunov coefficient according to Algorithm 2 and obtained that $\ell_1^N(\tau_c) = -9.65 \times 10^{-9}$, a very small but a negative value,[60] thus strongly indicative that the parameter regime of Fig. 6 in Ref. 49 lies at the edge of a supercritical Hopf bifurcation (for $\tau = \tau_c$).

The predicted supercritical Hopf bifurcation is confirmed by direct numerical integration of the KF model. Panel (a) of Fig. 13 shows indeed emergence of stable limit cycles whose amplitude grows as τ moves away from and above τ_c; stable limit cycles approximated to good accuracy from a 20D GK system for this parameter regime here; see the red dashed curve. Panel (b) of Fig. 13 shows the trajectories underlying the limit cycle shown for $\tau = 25.4$ in Panel (a) of Fig. 13, while indicating on the figure's axes the physical interpretation of the model's variables and units.

Note that a GK approximation is computed here from the KF model still written in the fluctuation variables about the critical equilibrium but without Taylor expansion, unlike in Sec. IV B. It consists just of replacing the nonlinearity in (65) by

$$\boldsymbol{F}(u(t-\tau), v(t-\tau)) = \begin{pmatrix} \dfrac{b-\bar{x}}{s_1} - \dfrac{a(\bar{x}+u(t-\tau))^2}{\bar{y}+v(t-\tau)} - \dfrac{a\bar{x}^2}{\bar{y}^2}v(t-\tau) + \dfrac{2a\bar{x}}{\bar{y}}u(t-\tau) \\ \dfrac{c-\bar{y}}{s_2} - d(\bar{x}+u(t-\tau))^3 + 3d\bar{x}^2\,u(t-\tau) \end{pmatrix}. \tag{82}$$

Then, the GK approximation is obtained by applying Algorithm 1 to Eq. (65) with $\boldsymbol{F}$ given by (82). The reason behind this remark is because unlike in Sec. IV B, the KF's solution exhibits a large amplitude in physical regimes, and thus, the Taylor approximation (64) is no longer a valid approximation. Nevertheless, GK systems such as (75) that are based on (65) with $\boldsymbol{F}$ given by (67) are perfectly valid to determine the Lyapunov coefficient $\ell_1^N(\tau_c)$, as the latter is computed at $\tau = \tau_c$, i.e., at the very onset of small amplitude oscillations; see Appendix B.

Section IV C taught us about the determining role of the nonlinear effects' intensity in the occurrence of either a super- or

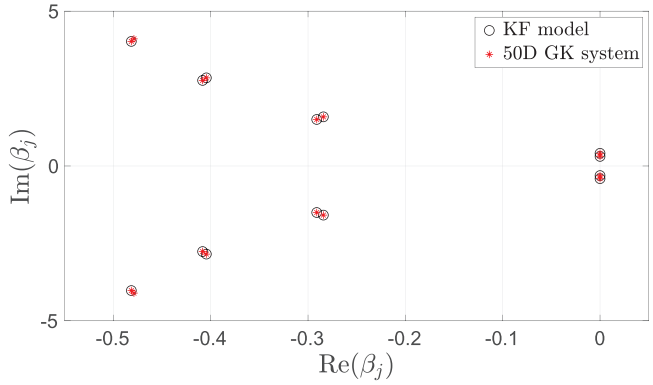

FIG. 12. Double-Hopf bifurcation: Spectral signature. Eigenvalues obtained from the KF model (black circles) linearized at the critical equilibrium vs the eigenvalues of Γ_N given in (76) with $N = 25$ (red asterisks). Here, these eigenvalues are computed for the parameter values corresponding to the jump observed on $\ell_1^N(\tau_c)$ in Fig. 11 for $d = 4.5$.

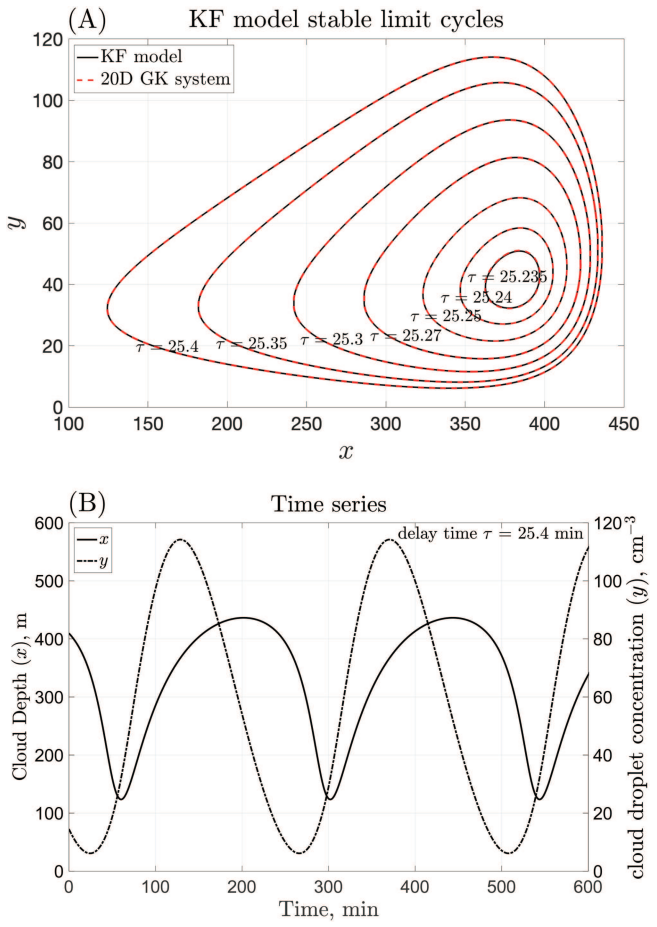

FIG. 13. Panel (a): KF model stable limit cycles as τ grows away from τ_c. Panel (b): KF model's trajectories for $\tau = 25.4$. The KF model's solutions and those to the corresponding GK approximations are obtained by using the solvers as described in Appendix C 3.

subcritical Hopf bifurcation. Thus, to understand the dependence of these nonlinear effects in the physical parameter regime considered here, we analyze the dependence of the Lyapunov coefficient on the coefficient a by computing the Lyapunov coefficient as a is varied within a small interval $I = [a_1, a_2]$ with $a_1 = 3.472 \times 10^{-4}$ and $a_2 = 0.02$.

The results are shown in Fig. 14. Panel (a) shows the dependence of the critical delay τ_c as a varies, while panel (b) shows the dependence of $\ell_1^N(\tau_c)$ in terms of the same parameter for $N = 50$. Similar to Fig. 11, we observe coexistence of supercritical and subcritical Hopf bifurcation intervals. A double-Hopf bifurcation is also identified for $a = a_\# = 86.5 \times 10^{-4}$ occurring at the jump discontinuity in the Lyapunov coefficient.[61]

Panel (c) shows magnification of the gray box in panel (b), in which we have indicated by a vertical black dashed line (crossing at $a^* = 6.9444 \times 10^{-4}$ the a-axis) the point in the parameter space corresponding to Fig. 6 in Ref. 49. Note that in Fig. 14, $\tau = \tau_c$ and not $\tau = 12$ as considered in Fig. 6 of Ref. 49. It confirms that the choice in Ref. 49 lies at the edge of a supercritical Hopf bifurcation region in the parameter space, on one hand, but also that the emergence of stable limit cycles is guaranteed (Theorem III.1) as τ moves away from τ_c; see also panel (a) in Fig. 13.

Finally, we emphasize that the prediction of subcritical Hopf bifurcations by our Lyapunov coefficient analysis relying on a 20D GK approximation, is actually quite accurate, including for subcritical Hopf regimes with small positive values of the Lyapunov coefficient. To illustrate this, we consider the case $a = 0.8a^*$, keeping the other model's coefficients as in Fig. 14. The corresponding Lyapunov coefficient is $\ell_1^N(\tau_c) = 4.47 \times 10^{-8}$, and indeed, this parameter regime is characterized by the emergence of unstable periodic orbits (UPOs) as τ decreases from $\tau_c = 20.844$; see panel (a) in Fig. 15.

For this parameter regime and given a τ-value, these UPOs are computed from the 20D GK approximation of the full KF model (i.e., without Taylor approximation of the nonlinearity). Techniques to compute UPOs for high-dimensional ODE systems are available; see, e.g., Ref. 62 and references therein. For our purpose, it was sufficient to compute these UPOs by using the Matlab built-in function `bvp4c` in order to solve the corresponding boundary problems.

TABLE II. Physical parameter regime.

a	b	c	d	s_1	s_2
6.9444×10^{-4}	530	180	4.1667×10^{-8}	60	60

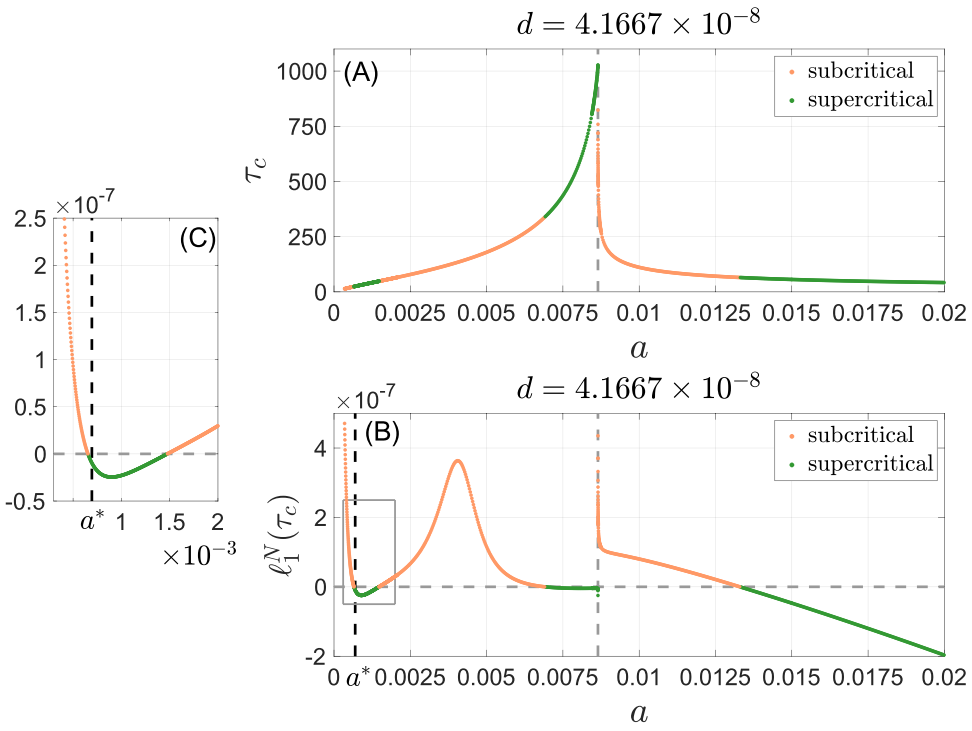

FIG. 14. Panel (a): Parameter dependence on a of the critical delay parameter τ_c for the KF model (60), with the parameter d set to be $d = 6 \times 10^{-5}/(24 \times 60) \approx 4.1667 \times 10^{-8}$ and all other parameters given in Table II. Panel (b): Same but for the Lyapunov coefficient $\ell_1^N(\tau_c)$ given by (40) for $N = 50$. The vertical black dashed line corresponds to $a = a^* = 1/(24 \times 60)$, which is the value used in Fig. 6 of Ref. 49. The vertical gray dashed line corresponds to a double-Hopf bifurcation occurring at $a_\# = 86.5 \times 10^{-4}$. Panel (c): A zoom of the $\ell_1^N(\tau_c)$-curve over the interval of a marked by the gray box in Panel (b). The mesh size of a used to produce this figure is $\delta a \approx 1.3 \times 10^{-5}$, with further local refinement near the jump of the Lyapunov coefficient $\ell_1^N(\tau_c)$. Note the use of a higher-dimensional GK system ($N = 50$) for the computations underlying this figure compared to those underlying Figs. 13 and 15 ($N = 20$) for the same physical parameter regime. This choice is made here to ensure a high-precision approximation of the corresponding Lyapunov coefficient as one approaches degeneracy, i.e., as a gets close to $a_\#$, at which the double-Hopf bifurcation takes place. In particular, the degeneracy location is approximated up to a precision 10^{-9} (see Ref. 61).

However, to be successful, the initial guess has to be selected with care as in any UPO algorithms.

Here, we rely on our theoretical predictions to choose the initial guess to properly initiate the UPO algorithm for the 20D GK system. First, for $\tau = 20.6$, an initial guess is chosen to be given by the analytic approximation to the unstable periodic solution of the Stuart–Landau Eq. (36) whose amplitude and period are given by Remark III.1. This initial guess is used then to determine the UPO for the corresponding 2D CM reduced equation. The latter reduced equation is given as for the KTF model by (52) but this time with the $F_N^{(2)}$-term given by (B4) ($N = 10$) and the spectral elements required to determine the CM approximation Φ_2 [see (A55)] to be those of $\Gamma_N(\tau)$ given by (76). Once the UPO for $\tau = 20.6$ is obtained according to this strategy, it is used as an initial guess in `bvp4c` to determine the UPO of the corresponding GK system for the next (larger) τ-value and so forth (up to $\tau = 20.83$).

The unstable character of these UPOs, obtained from 20D GK approximations, is then illustrated for the full KF model in panels (b)–(d) of Fig. 15 for $\tau = 20.6$. There, we show a KF model's trajectory $x(t)$ (solid black curves) that starts close to the UPO, $\gamma(t)$, (dashed curve) and experiences a slow divergence from it to converge eventually toward the non-trivial steady state; the long oscillatory transient is being dominated by an oscillation "period" of about $T(\lambda)$ given in (41), with $\lambda = \tau$. This slow divergence observed when starting close to such UPOs obtained from the 20D GK approximation strongly suggests that these UPOs approximate accurately the genuine KF model's UPOs for $a = 0.8a^*$.

These numerical results are complemented by cross-checking with the DDE-BIFTOOL software. The accuracy of the computed limit cycles reported in panel (a) of Fig. 13 and panel (a) of Fig. 15 has been further checked by comparing those obtained with DDE-BIFTOOL;[21] the relative L^2-error over one period turned out to be always below 0.3% for all the limit cycles reported in Figs. 13 and 15. Tables III and IV report on the (nontrivial) dominant Floquet multiplier as computed from DDE-BIFTOOL for each limit cycles shown in panel (a) of Fig. 13 and panel (a) of Fig. 15. In each case, the dominant Floquet multiplier (determining stability of the limit cycle) has a value close to one, indicating either a slow relaxation toward the stable limit cycle in the supercritical Hopf case (Fig. 13) or a slow deviation from the unstable limit cycle in the subcritical Hopf case (Fig. 15), confirming the aforementioned numerical observations; see panels (b)–(d) of Fig. 15 and Appendix C 4.

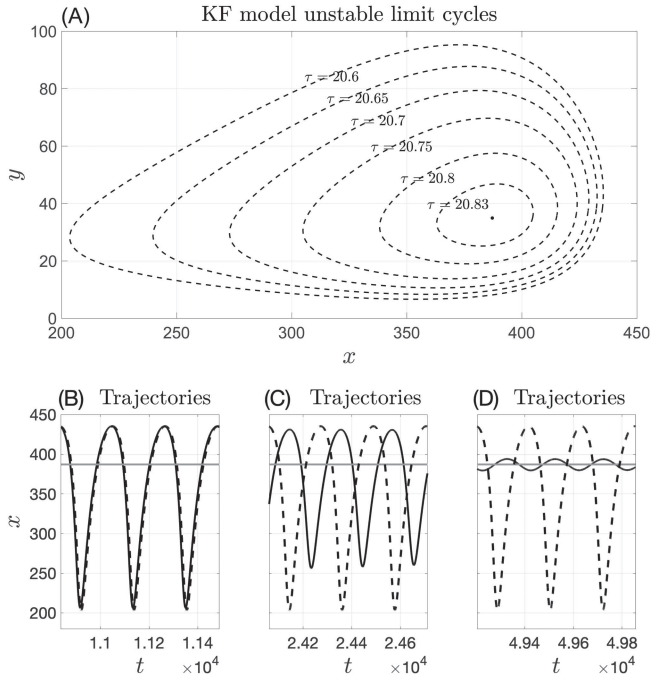

FIG. 15. Panel (a): Approximation of the KF model's unstable limit cycles as τ decreases away from $\tau_c \approx 20.844$. These unstable periodic orbits (UPOs) are obtained from the 20D GK approximation of the KF model. Panels (b)–(d): KF model's trajectory $x(t)$ (solid black curves) over consecutive but distant time windows for $\tau = 20.6$ and emanating from an initial history ϕ taken to be $\phi(\theta) = \gamma(\theta) - 0.01\,(\theta \in (-\tau, 0))$, where $\gamma(t)$ denotes the corresponding UPO. The latter is shown as a dashed curve over the time windows. As time evolves, the KF model's solution eventually settles down, through a very slow oscillatory transient regime, toward the non-trivial steady state, which is marked by the horizontal gray lines. The parameters are those of Table II except that $a = 0.8a^*$ with a^* given in the caption of Fig. 14. For this choice of a, the Lyapunov coefficient at τ_c is 4.47×10^{-8}.

TABLE III. The (nontrivial) dominant Floquet multiplier μ: Supercritical Hopf case ($a = a^*$).

τ	25.235	25.24	25.25	25.27	25.30	25.35	25.40
μ	0.9996	0.9989	0.9972	0.9928	0.9837	0.9646	0.9482

TABLE IV. The dominant Floquet multiplier μ: Subcritical Hopf case ($a = 0.8a^*$).

τ	20.60	20.65	20.70	20.75	20.80	20.83
μ	1.060	1.045	1.032	1.019	1.008	1.002

V. CONCLUSION

In this article, we proposed a simple analytic approach to characterize the type of Hopf bifurcation in a broad class of nonlinear systems of DDEs including the case of discrete delays and distributed delays. It consists of first approximating the DDEs by ODE systems constructed from the rigorous Galerkin–Koornwinder (GK) method introduced in Ref. 26 and then applying the center-manifold approximation techniques to the leading order[37] followed by the normal form theory for ODEs. The nature of the associated Hopf bifurcation (super- or subcritical) is then characterized by the sign of a Lyapunov coefficient (40) obtained within this framework and easy to determine based on the model's coefficients and delay parameters. Applications to cloud-rain models including the KTF model and the KF model are discussed in detail in which super- and subcritical bifurcations are shown to coexist for the latter; see Secs. III B, III C, and IV, respectively. New dynamical behaviors are exhibited for such models such as double-Hopf bifurcations, and new dynamical insights about the physical regimes are discussed.

As a concluding remark, we would like to emphasize that, in spite of multiple theoretical as well as numerical evidences shown here, some authors have incorrectly apprehended the non-existence of limit cycles in the KF model, eventually leading them to conclude to a somewhat absolute non-existence of limit cycles in the KF model.[63] Their conclusion is in contradiction with the numerous Hopf bifurcations occurring in this model depending on the parameter regimes, as shown in Secs. IV B–IV D. Perhaps, it is their numerical treatment of delay equations[64] conjugated to their incorrect application of the Busenberg–van den Driessche theorem[65] about nonexistence of closed orbits—which are simple loop solutions—in higher-dimensional spaces. To be brief, Theorem 4.1 in Ref. 65 provides conditions to exclude the existence of periodic, *simple loop*,[66] solutions to a DDE system. The results of Ref. 65 are, however, insufficient to rule out the existence of periodic solutions for DDE systems, as the authors of Ref. 65 pointed out themselves [see comments after (4.8) therein]. It does not preclude the existence of periodic solutions that indeed self-intersect in the (x, y)-plane. Such solutions are perfectly admissible for DDEs due to their infinite-dimensional setting. They are encountered for the KF model as produced from either a supercritical or subcritical Hopf bifurcation such as shown in Figs. 5 and 10.

What is about the simple loop solutions for the KF model then? As predicted by Theorem III.1, panel (a) of Fig. 13 shows stable limit cycles of the KF model, which are (clockwise) simple loops, incompatible with the claim in Ref. 63. Essentially, the flaw in Ref. 63 lies in the verification of condition (4.3) in Theorem 4.1 of Ref. 65. The latter provides a sufficient condition to the non-existence of periodic, simple loop solutions, which, unlike the Bendixson–Dulac theorem for planar ODEs (consequence of the Green's theorem), is evaluated along the periodic orbit $X(t)$ to be excluded. As pointed out in example (4.5) after Corollary 4.2 in Ref. 65, it is for very specific balance relationships between the linear terms and the coefficients in front of the (nonlinear) delay terms that one can check condition (4.3) in Theorem 4.1 of Ref. 65 [without having to know $X(t)$] to conclude to the non-existence of simple loop solutions. In more general situations in which the KF model falls, the checking of condition (4.3) in

Theorem 4.1 of Ref. 65 is more delicate, and this condition becomes less useful for DDEs.

Based on the analysis of cloud-rain delay models conducted here, especially their analytic reduction to Stuart–Landau oscillators, we envision a further program, relevant for cloud dynamics, of analyzing spatiotemporal patterns arising in a ring of delayed-coupled oscillators along with the study of the oscillation quenching phenomenon for such models.[67,68]

In cloud physics, special attention is paid to the transition between closed and open cellular convection.[49,69,70] In mathematical terms, a cloud system near its bifurcation point (associated with a closed-open transition) is particularly important to study. We demonstrated that the GK approach combined with the center-manifold reduction allows us to replace the original system of DDEs with, here, a simpler system of two coupled ODEs (near the Hopf bifurcation) that captures essential dynamics and physics. By exploiting such analytical insights, we believe that the framework introduced in this article offers promising perspectives to further progress in the understanding of the transitions between open and closed cells.

ACKNOWLEDGMENTS

We are grateful to the anonymous reviewers for their valuable suggestions and insightful comments. This work has been partially supported by the European Research Council (ERC) under the European Union's Horizon 2020 research and innovation program [Grant Agreement No. 810370 (M.D.C. and I.K.)] and by the U.S. National Science Foundation (NSF) [Grant No. DMS-1616450 (H.L.)].

DATA AVAILABILITY

The data that support the findings of this study are available from the corresponding author upon reasonable request.

APPENDIX A: KOORNWINDER POLYNOMIALS AND USEFUL PROPERTIES TO APPROXIMATE DDEs

1. 1D Koornwinder polynomials

Koornwinder polynomials K_n have been introduced in Ref. 27. They are obtained from Legendre polynomials L_n according to the relation [see Eq. (2.1) in Ref. 27]

$$K_n(s) = -(1+s)\frac{\mathrm{d}}{\mathrm{d}s}L_n(s) + (n^2+n+1)L_n(s), \quad s \in [-1,1],\ n \in \mathbb{N}. \tag{A1}$$

Koornwinder polynomials are known to form an orthogonal set for the following weighted inner product with a point mass on $[-1,1]$:

$$\mu(\mathrm{d}x) = \frac{1}{2}\,\mathrm{d}x + \delta_1, \tag{A2}$$

where δ_1 denotes the Dirac point mass at the right end point $x = 1$; see Ref. 27. In other words,

$$\int_{-1}^{1} K_n(s)K_p(s)\,\mathrm{d}\mu(s) = \frac{1}{2}\int_{-1}^{1} K_n(s)K_p(s)\,\mathrm{d}s + K_n(1)K_p(1) = 0 \text{ if } p \neq n. \tag{A3}$$

The following polynomials, $\mathcal{K}_n$, constituted by the K_n's to which a point value has been added:

$$\mathcal{K}_n = (K_n, K_n(1)), \tag{A4}$$

form an orthogonal basis of the following product space:

$$\mathcal{E} = L^2([-1,1);\mathbb{R}) \times \mathbb{R}, \tag{A5}$$

where $\mathcal{E}$ is endowed with the following inner product:

$$\langle (f,a),(g,b)\rangle_{\mathcal{E}} = \frac{1}{2}\int_{-1}^{1} f(s)g(s)\,\mathrm{d}s + ab, \quad (f,a),(g,b) \in \mathcal{E}. \tag{A6}$$

The norm induced by this inner product is denoted hereafter by $\|\cdot\|_{\mathcal{E}}$. It is shown then in Proposition 3.1 of Ref. 26 that the norm of the basis function $\mathcal{K}_n$ is given by

$$\|\mathcal{K}_n\|_{\mathcal{E}} = \sqrt{\frac{(n^2+1)((n+1)^2+1)}{2n+1}}, \quad n \in \mathbb{N}. \tag{A7}$$

We now explain how the sequence $\mathcal{K}_n$ is rescaled to form a basis of the following Hilbert space:

$$\mathcal{H}_1 = L^2([-\tau,0);\mathbb{R}) \times \mathbb{R}, \tag{A8}$$

endowed with the inner product defined for any (f_1,x_1), (f_2,x_2) in $\mathcal{H}_1$, as

$$\langle (f_1,x_1),(f_2,x_2)\rangle_{\mathcal{H}_1} = \frac{1}{\tau}\int_{-\tau}^{0} f_1(\theta)f_2(\theta)\,\mathrm{d}\theta + x_1x_2. \tag{A9}$$

The original Koornwinder polynomials are defined on $[-1,1]$. We define now on $[-\tau,0]$ the following rescaled Koornwinder polynomials:

$$K_n^\tau(\theta) = K_n\left(1 + \frac{2\theta}{\tau}\right), \quad \theta \in [-\tau,0]. \tag{A10}$$

Consider now the following version of the $\mathcal{K}_n$'s given by (A4) including a point value at $\theta = 0$ but now defined on $[-\tau,0]$:

$$\mathcal{K}_n^\tau(\theta) = (K_n^\tau(\theta), K_n^\tau(0)), \quad \theta \in [-\tau,0]. \tag{A11}$$

As shown in Ref. 26, the $\mathcal{K}_n^\tau$'s form an orthogonal basis of the Hilbert space $\mathcal{H}_1 = L^2([-\tau,0);\mathbb{R}) \times \mathbb{R}$ endowed with the inner product $\langle\cdot,\cdot\rangle_{\mathcal{H}_1}$ given in (A9). Note that since $K_n(1) = 1$ (Proposition 3.1 in Ref. 26), we have

$$K_n^\tau(0) = 1. \tag{A12}$$

Note also that

$$\|\mathcal{K}_n^\tau\|_{\mathcal{H}_1} = \|\mathcal{K}_n\|_{\mathcal{E}} = \sqrt{\frac{(n^2+1)((n+1)^2+1)}{2n+1}}, \quad n \in \mathbb{N}. \tag{A13}$$

Then, Lemma 3.1 in Ref. 26 provides key properties of Koornwinder polynomials used to provide Galerkin approximations of

scalar DDEs. In particular, for any function f in $L^2([-\tau,0];\mathbb{R})$, the following expansion formula holds:

$$f(\theta)=\sum_{j=0}^{\infty}\frac{\langle f,K_j^\tau\rangle_{L^2}}{\tau\|K_j^\tau\|_{\mathcal{H}}^2}K_j^\tau(\theta),\quad \theta\in[-\tau,0]. \tag{A14}$$

Similarly, any element $\psi=(f,x)$ of $\mathcal{H}_1$ possesses the following decomposition:

$$\begin{aligned}\psi(\theta)&=\sum_{j=0}^{\infty}\frac{\langle\psi,\mathcal{K}_j^\tau\rangle_{\mathcal{H}_1}}{\|\mathcal{K}_j^\tau\|_{\mathcal{H}_1}^2}\mathcal{K}_j^\tau(\theta)\\&=\sum_{j=0}^{\infty}\left(\frac{1}{\tau}\langle\psi,K_j^\tau\rangle_{L^2}+xK_j^\tau(0)\right)\frac{\mathcal{K}_j^\tau(\theta)}{\|\mathcal{K}_j^\tau\|_{\mathcal{H}_1}^2},\quad \theta\in[-\tau,0].\end{aligned} \tag{A15}$$

2. The Koornwinder derivative matrix T

In the derivation of analytic formulas of GK systems, it is key to express the derivative of Koornwinder polynomials in terms of the polynomials themselves. We recall this result below and refer to Appendix B in Ref. 26 for a proof.

Proposition A.1: *The Koornwinder polynomial K_n of degree $n\geq 1$ defined in (A1) satisfies the differential relation,*

$$\frac{\mathrm{d}K_n}{\mathrm{d}s}(s)=\sum_{k=0}^{n-1}a_{n,k}K_k(s),\quad s\in(-1,1), \tag{A16}$$

where the coefficients $\boldsymbol{a}_n=(a_{n,0},\ldots,a_{n,n-1})^T$ satisfy the upper triangular system of linear equations,

$$\mathbf{T}\boldsymbol{a}_n=\boldsymbol{b}_n, \tag{A17}$$

with $\mathbf{T}=(\mathbf{T}_{i,j})_{n\times n}$ and $\boldsymbol{b}_n=(b_{n,0},\ldots,b_{n,n-1})^T$ given by

$$\mathbf{T}_{i,j}=\begin{cases}0 & \text{if } j<i,\\ i^2+1 & \text{if } j=i,\\ -(2i+1) & \text{if } j>i,\end{cases}\quad \text{where}\quad 0\leq i,j\leq n-1, \tag{A18}$$

$$b_{n,i}=\begin{cases}\frac{1}{2}(2i+1)(n+i+1)(n-i) & \text{if } n+i \text{ is even},\\ (n^2+n)(2i+1)-\frac{i}{2}(n+i)(n-i+1)-\frac{i}{2}(i+1)(n-i-1)(n+i+2) & \text{if } n+i \text{ is odd}.\end{cases}$$

For the rescaled version K_n^τ defined by (A10), it holds that

$$\frac{\mathrm{d}K_n^\tau}{\mathrm{d}\theta}(\theta)=\frac{2}{\tau}\sum_{k=0}^{n-1}a_{n,k}K_k^\tau(\theta),\quad n\in\mathbb{N},\quad \theta\in(-\tau,0). \tag{A19}$$

The matrix $\mathbf{T}$ is referred to as the Koornwinder derivative matrix $\mathbf{T}$.

3. Approximation space for DDE systems by vectorization of Koornwinder polynomials

Following Ref. 26, we introduce vectorization of Koornwinder polynomials for the purpose of providing analytic, finite-dimensional approximations of nonlinear DDE systems. For this purpose, we recall below how scalar Koornwinder polynomials are used to form a basis of the Hilbert space of vector-valued functions,

$$\mathcal{H}_d=L^2([-\tau,0);\mathbb{R}^d)\times\mathbb{R}^d, \tag{A20}$$

when the latter is endowed with the inner product defined for any (f_1,x_1) and (f_2,x_2) in $\mathcal{H}_d$ by

$$\langle(f_1,x_1),(f_2,x_2)\rangle_{\mathcal{H}_d}=\frac{1}{\tau}\int_{-\tau}^{0}\langle f_1(\theta),f_2(\theta)\rangle\mathrm{d}\theta+\langle x_1,x_2\rangle. \tag{A21}$$

Here, $\langle\cdot,\cdot\rangle$ denotes the Euclidean inner product of $\mathbb{R}^d$.

The purpose is to build from the scalar Koornwinder polynomials introduced above, linear subspaces $\mathcal{H}_N$ that approximate $\mathcal{H}_d$. To do so, given $1\leq j\leq Nd$, we consider the following integer decomposition:

$$j=dj_q+j_r, \tag{A22}$$

in which $0\leq j_q\leq N-1$ and $1\leq j_r\leq d$ are determined according to

$$j_r=\begin{cases}\mathrm{mod}(j,d) & \text{if } \mathrm{mod}(j,d)\neq 0,\\ d, & \text{otherwise.}\end{cases} \tag{A23}$$

Given an integer $1\leq j\leq Nd$, the integer pair (j_q,j_r) is used to construct the following sparse $\mathbb{R}^d$-valued vector, whose only non-zero entry is the j_rth-entry given by the (rescaled) Koornwinder polynomial of degree j_q, namely,

$$\mathbf{K}_j^\tau(\theta)=(\underbrace{0,\ldots,0}_{j_r-1\text{ entries}},K_{j_q}^\tau(\theta),\underbrace{0,\ldots,0}_{d-j_r\text{ entries}})^{\mathrm{T}},\quad \theta\in[-\tau,0]. \tag{A24}$$

Based on these vectorized (rescaled) Koornwinder polynomials $\mathbf{K}_j^\tau$, we finally introduce

$$\mathbb{K}_j^\tau(\theta)=\left(\mathbf{K}_j^\tau(\theta),\mathbf{K}_j^\tau(0)\right),\quad j\geq 1. \tag{A25}$$

$\mathbb{K}_j^\tau$ is the d-dimensional version of $\mathcal{K}_n^\tau$ defined above. Also of interest [see (30)] is the unrescaled vectorized Koornwinder polynomials $\mathbf{K}_j$ defined exactly as in (A24) but for θ in $[-1,1]$.

Each element $\Psi=(\psi_1,\ldots,\psi_d)$ in $\mathcal{H}_d$ has each of its components, ψ_j, that lies in $\mathcal{H}_1$, and therefore, each ψ_j is decomposed as a

series of Koornwinder polynomials according to (A15). Our approximation space is thus $\mathcal{H}_N \subset \mathcal{H}_d$ obtained as spanned by the first Nd vectorized Koornwinder polynomials introduced in (A25), namely,

$$\mathcal{H}_N = \operatorname{span}\left\{\mathbb{K}_1^\tau, \ldots, \mathbb{K}_{Nd}^\tau\right\}. \tag{A26}$$

Since the $\mathcal{K}_j^\tau$'s form an orthogonal basis of $\mathcal{H}_1$, the vector-valued polynomials $\mathbb{K}_j^\tau$'s are orthogonal for the inner product with a point mass defined in (A21). Note also that

$$\|\mathbb{K}_j^\tau\|_{\mathcal{H}_d} = \|\mathcal{K}_{j_q}^\tau\|_{\mathcal{H}_1}, \quad j \geq 1. \tag{A27}$$

Then, Lemma 3.2 in Ref. 26 provides key properties of the $\mathbf{K}_j^\tau$'s and $\mathbb{K}_j^\tau$'s used for the rigorous approximation of nonlinear systems of DDEs. In particular, for any function $\boldsymbol{f}$ in $L^2([-\tau, 0]; \mathbb{R}^d)$, the following expansion formula holds:

$$\boldsymbol{f}(\theta) = \sum_{j=1}^{\infty} \frac{\langle \boldsymbol{f}, \mathbf{K}_j^\tau \rangle_{L^2}}{\tau \|\mathcal{K}_{j_q}^\tau\|_{\mathcal{H}_1}^2} \mathbf{K}_j^\tau(\theta), \quad \theta \in [-\tau, 0]. \tag{A28}$$

4. Derivation of the GK system (26)

In this appendix, we provide details about how the GK system (26) is derived from (25). The main calculation consists of making explicit the term $\langle \mathcal{A}_N \mathbb{K}_n^\tau, \mathbb{K}_j^\tau \rangle_{\mathcal{H}_d}$. Since $\mathcal{A}_N = \Pi_N \mathcal{A} \Pi_N$ according to (22) and $\mathbb{K}_n^\tau$ is an element in $\mathcal{H}_N$ for all $n \leq Nd$, we obtain thus $\mathcal{A}_N \mathbb{K}_n^\tau = \Pi_N \mathcal{A} \Pi_N \mathbb{K}_n^\tau = \Pi_N \mathcal{A} \mathbb{K}_n^\tau$. We get then for $1 \leq n, j \leq Nd$,

$$\langle \mathcal{A}_N \mathbb{K}_n^\tau, \mathbb{K}_j^\tau \rangle_{\mathcal{H}_d} = \langle \Pi_N \mathcal{A} \mathbb{K}_n^\tau, \mathbb{K}_j^\tau \rangle_{\mathcal{H}_d} = \langle \mathcal{A} \mathbb{K}_n^\tau, \mathbb{K}_j^\tau \rangle_{\mathcal{H}_d}, \tag{A29}$$

where the last identity above holds because $\mathbb{K}_j^\tau$ is an element in $\mathcal{H}_N$ when j is less than or equal to Nd.

By using the definitions of $\mathcal{A}$ and $\mathbb{K}_n^\tau$ given, respectively, by (17) and (A25), we have

$$\mathcal{A}\mathbb{K}_n^\tau = \begin{cases} \dfrac{\mathrm{d}\mathbf{K}_n^\tau(\theta)}{\mathrm{d}\theta}, & \theta \in [-\tau, 0), \\ L\mathbf{K}_n^\tau(0) + B\mathbf{K}_n^\tau(-\tau) + C\displaystyle\int_{-\tau}^{0} \mathbf{K}_n^\tau(s)\,\mathrm{d}s, & \theta = 0. \end{cases} \tag{A30}$$

It follows then by applying (A21) that

$$\begin{aligned} \langle \mathcal{A}\mathbb{K}_n^\tau, \mathbb{K}_j^\tau \rangle_{\mathcal{H}_d} = {} & \frac{1}{\tau} \int_{-\tau}^{0} \left\langle \frac{\mathrm{d}\mathbf{K}_n^\tau(\theta)}{\mathrm{d}\theta}, \mathbf{K}_j^\tau(\theta) \right\rangle \mathrm{d}\theta \\ & + \left\langle L\mathbf{K}_n^\tau(0) + B\mathbf{K}_n^\tau(-\tau) + C\int_{-\tau}^{0} \mathbf{K}_n^\tau(s)\,\mathrm{d}s, \mathbf{K}_j^\tau(0) \right\rangle. \end{aligned} \tag{A31}$$

By definition of (A24), we have

$$\left\langle \frac{\mathrm{d}\mathbf{K}_n^\tau(\theta)}{\mathrm{d}\theta}, \mathbf{K}_j^\tau(\theta) \right\rangle = \left(\frac{\mathrm{d}K_{n_q}^\tau(\theta)}{\mathrm{d}\theta} \right) K_{j_q}^\tau(\theta) \delta_{n_r, j_r}, \tag{A32}$$

which leads to [cf. (A19)]

$$\left\langle \frac{\mathrm{d}\mathbf{K}_n^\tau(\theta)}{\mathrm{d}\theta}, \mathbf{K}_j^\tau(\theta) \right\rangle = \frac{2}{\tau} \left(\sum_{k=0}^{n_q - 1} a_{n_q, k} K_k^\tau(\theta) \right) K_{j_q}^\tau(\theta)\, \delta_{n_r, j_r}. \tag{A33}$$

As a result,

$$I_{n,j}(\tau) = \frac{1}{\tau} \int_{-\tau}^{0} \left\langle \frac{\mathrm{d}\mathbf{K}_n^\tau(\theta)}{\mathrm{d}\theta}, \mathbf{K}_j^\tau(\theta) \right\rangle \mathrm{d}\theta$$

satisfies

$$I_{n,j}(\tau) = \frac{2}{\tau} \left(\sum_{k=0}^{n_q - 1} a_{n_q, k} \left(\frac{1}{\tau} \int_{-\tau}^{0} K_k^\tau(\theta) K_{j_q}^\tau(\theta)\,\mathrm{d}\theta \right) \right) \delta_{n_r, j_r}. \tag{A34}$$

Recall from (A11) that $\mathcal{K}_n^\tau = (K_n^\tau, K_n^\tau(0))$. Recall also the inner product $\langle \cdot, \cdot \rangle_{\mathcal{H}_1}$ given by (A9) and $K_n^\tau(0) = 1$ for all n as given by (A12). We have then that all ℓ and $m \geq 0$,

$$\begin{aligned} \frac{1}{\tau} \int_{-\tau}^{0} K_\ell^\tau(\theta) K_m^\tau(\theta)\,\mathrm{d}\theta &= \langle \mathcal{K}_\ell^\tau, \mathcal{K}_m^\tau \rangle_{\mathcal{H}_1} - 1 \\ &= \delta_{m,\ell} \|\mathcal{K}_m^\tau\|_{\mathcal{H}_1}^2 - 1, \end{aligned} \tag{A35}$$

recalling that $\{\mathcal{K}_k^\tau\}$ forms an orthogonal basis of $\mathcal{H}_1$; see Appendix A 1.

Now, using (A35) in (A34) and recalling from (A13) that $\|\mathcal{K}_n^\tau\|_{\mathcal{H}_1} = \|\mathcal{K}_n\|_{\mathcal{E}}$, we obtain finally

$$I_{n,j}(\tau) = \frac{2}{\tau} \left(\sum_{k=0}^{n_q - 1} a_{n_q, k} \left(\delta_{j_q, k} \|\mathcal{K}_{j_q}\|_{\mathcal{E}}^2 - 1 \right) \right) \delta_{n_r, j_r}. \tag{A36}$$

For the second term on the RHS of (A31), note that $\mathbf{K}_j^\tau(0)$ and $\mathbf{K}_n^\tau(0)$ are simply the j_r-th and the n_r-th canonical vectors of $\mathbb{R}^d$, respectively; see again (A24) and (A12). Denoting the canonical vectors of $\mathbb{R}^d$ by $\{\boldsymbol{f}_k\}_{k=1}^d$, we thus have

$$\begin{aligned} \left\langle L\mathbf{K}_n^\tau(0), \mathbf{K}_j^\tau(0) \right\rangle &= \left\langle L\boldsymbol{f}_{n_r}, \boldsymbol{f}_{j_r} \right\rangle \\ &= (\boldsymbol{f}_{j_r})^{\mathrm{T}} L \boldsymbol{f}_{n_r} = L_{j_r, n_r}. \end{aligned} \tag{A37}$$

Similarly, since $\mathbf{K}_n^\tau(-\tau) = K_{n_q}^\tau(-\tau)\boldsymbol{f}_{n_r}$ and $K_{n_q}^\tau(-\tau) = K_{n_q}(-1)$ thanks to (A10), we have

$$\begin{aligned} \left\langle B\mathbf{K}_n^\tau(-\tau), \mathbf{K}_j^\tau(0) \right\rangle &= K_{n_q}(-1)(\boldsymbol{f}_{j_r})^{\mathrm{T}} B \boldsymbol{f}_{n_r} \\ &= K_{n_q}(-1) B_{j_r, n_r}. \end{aligned} \tag{A38}$$

For $\langle C \int_{-\tau}^{0} \mathbf{K}_n^\tau(s)\,\mathrm{d}s, \mathbf{K}_j^\tau(0) \rangle$, since

$$\begin{aligned} \int_{-\tau}^{0} \mathbf{K}_n^\tau(s)\,\mathrm{d}s &= \int_{-\tau}^{0} K_{n_q}^\tau(s)\,\mathrm{d}s\, \mathbf{K}_n^\tau(0) \\ &= \int_{-\tau}^{0} K_{n_q}^\tau(s)\,\mathrm{d}s \boldsymbol{f}_{n_r}, \end{aligned} \tag{A39}$$

we have

$$\begin{aligned} \left\langle C\int_{-\tau}^{0} \mathbf{K}_n^\tau(s)\,\mathrm{d}s, \mathbf{K}_j^\tau(0) \right\rangle &= \int_{-\tau}^{0} K_{n_q}^\tau(s)\,\mathrm{d}s\, \langle C\boldsymbol{f}_{n_r}, \boldsymbol{f}_{j_r} \rangle \\ &= C_{j_r, n_r} \int_{-\tau}^{0} K_{n_q}^\tau(s)\,\mathrm{d}s. \end{aligned} \tag{A40}$$

Using again (A35) and $K_0^\tau \equiv 1$, we obtain

$$\int_{-\tau}^{0} K_{n_q}^\tau(s)\,\mathrm{d}s = \int_{-\tau}^{0} K_0^\tau(s) K_{n_q}^\tau(s)\,\mathrm{d}s = \tau\left(\delta_{n_q,0}\|\mathcal{K}_0^\tau\|_{\mathcal{H}_1}^2 - 1\right) = \tau\left(2\delta_{n_q,0} - 1\right), \tag{A41}$$

where the last equality follows from $\|\mathcal{K}_0^\tau\|_{\mathcal{H}_1}^2 = 2$.

Summarizing (A37) and (A38) and (A40) and (A41), we obtain

$$\left\langle L\mathbf{K}_n^\tau(0) + B\mathbf{K}_n^\tau(-\tau) + C\int_{-\tau}^{0}\mathbf{K}_n^\tau(s)\,\mathrm{d}s,\ \mathbf{K}_j^\tau(0)\right\rangle = L_{j_r,n_r} + K_{n_q}(-1)B_{j_r,n_r} + \tau\left(2\delta_{n_q,0} - 1\right)C_{j_r,n_r}. \tag{A42}$$

Finally, by using (A36) and (A42) in (A31), together with the identity $\langle \mathcal{A}_N\mathbb{K}_n^\tau, \mathbb{K}_j^\tau\rangle_{\mathcal{H}_d} = \langle \mathcal{A}\mathbb{K}_n^\tau, \mathbb{K}_j^\tau\rangle_{\mathcal{H}_d}$ derived in (A29), we obtain, for all $1 \le j, n \le Nd$, that

$$\langle \mathcal{A}_N\mathbb{K}_n^\tau, \mathbb{K}_j^\tau\rangle_{\mathcal{H}_d} = I_{n,j}(\tau) + L_{j_r,n_r} + K_{n_q}(-1)B_{j_r,n_r} + \tau\left(2\delta_{n_q,0} - 1\right)C_{j_r,n_r}. \tag{A43}$$

For the inner products, $\left\langle \mathcal{F}\left(\sum_{n=1}^{Nd} y_n(t)\mathbb{K}_n^\tau\right), \mathbb{K}_j^\tau\right\rangle_{\mathcal{H}_d}$ in (25), involving the nonlinear term $\mathcal{F}$ given by (16), we have, since $\mathbf{K}_j^\tau(0) = \boldsymbol{f}_{j_r}$,

$$\begin{aligned}\left\langle \mathcal{F}\left(\sum_{n=1}^{Nd} y_n(t)\mathbb{K}_n^\tau\right), \mathbb{K}_j^\tau\right\rangle_{\mathcal{H}_d} &= \left\langle \mathbf{F}\left(\sum_{n=1}^{Nd} y_n(t)\mathbf{K}_n^\tau(0), \sum_{n=1}^{Nd} y_n(t)\mathbf{K}_n^\tau(-\tau), \gamma(\tau)\right), \mathbf{K}_j^\tau(0)\right\rangle \\ &= \mathbf{F}_{j_r}\left(\sum_{n=1}^{Nd} y_n(t)\mathbf{K}_n^\tau(0), \sum_{n=1}^{Nd} y_n(t)\mathbf{K}_n^\tau(-\tau), \gamma(\tau)\right),\end{aligned}$$

with

$$\gamma(\tau) = \int_{-\tau}^{0}\sum_{n=1}^{Nd} y_n(t)\mathbf{K}_n^\tau(s)\,\mathrm{d}s.$$

By noting that $\mathbf{K}_n^\tau(0) = \mathbf{K}_n(1)$, $\mathbf{K}_n^\tau(-\tau) = \mathbf{K}_n(-1)$ and $\int_{-\tau}^{0}\mathbf{K}_n^\tau(s)\mathrm{d}s = \tau\left(2\delta_{n_q,0} - 1\right)\mathbf{K}_n(1)$ [see (A39) and (A41)], we obtain finally that

$$\left\langle \mathcal{F}\left(\sum_{n=1}^{Nd} y_n(t)\mathbb{K}_n^\tau\right), \mathbb{K}_j^\tau\right\rangle_{\mathcal{H}_d} = \mathbf{F}_{j_r}\left(\sum_{n=1}^{Nd} y_n(t)\mathbf{K}_n(1), \sum_{n=1}^{Nd} y_n(t)\mathbf{K}_n(-1), \gamma(\tau)\right), \tag{A44}$$

with

$$\gamma(\tau) = \tau\sum_{n=1}^{Nd}\left(2\delta_{n_q,0} - 1\right)\mathbf{K}_n(1)y_n(t).$$

Now, the GK system (26) follows from (25) by using (A43) and (A44).

5. Proof of Theorem III.1

Proof. The result follows from center-manifold reduction techniques,[71–73] in particular, by using the formulas of Theorem 2 in Ref. 37, applied to the GK approximations together with the characterization of Hopf bifurcations for planar systems[30,56] based on the normal form theory.

Step 1. We first provide a brief review of the characterization for the case of the planar system. To this end, let us consider the following ODE in the complex plane with polynomial RHS:

$$\frac{\mathrm{d}z}{\mathrm{d}t} = \beta(\lambda)z + \sum_{\substack{i+j=2\\ i,j\ge 0}}^{3} a_{ij}z^i\bar{z}^j + o(\|z\|^4), \tag{A45}$$

where $\beta(\lambda)$ and a_{ij} lie in $\mathbb{C}$, while λ is a real scalar parameter. To put into perspective of Hopf bifurcations, we assume that there exists some critical parameter value λ_c verifying [cf. Theorems 3.3 and 3.4 in Ref. 30]

$$\mathrm{Re}(\beta(\lambda_c)) = 0, \quad \mathrm{Im}(\beta(\lambda_c)) \neq 0, \quad \left[\frac{\mathrm{d}}{\mathrm{d}\lambda}\mathrm{Re}(\beta(\lambda))\right]\Big|_{\lambda=\lambda_c} > 0. \tag{A46}$$

We recall that the above equation (A45) can be rearranged into the following normal form:

$$\frac{\mathrm{d}w}{\mathrm{d}t} = \beta(\lambda)w + c(\lambda)w|w|^2 + o(|w|^3), \tag{A47}$$

where

$$c(\lambda) = \left(\frac{1}{\beta(\lambda)} + \frac{2}{\overline{\beta}(\lambda)}\right)a_{20}a_{11} + \frac{1}{\beta(\lambda)}|a_{11}|^2 + \frac{2}{2\beta(\lambda) - \overline{\beta}(\lambda)}|a_{02}|^2 + a_{21}. \tag{A48}$$

Note that this formula for $c(\lambda)$ may be obtained following, e.g., Ref. 30. More precisely, this formula is obtained from the formula of c_1 in Ref. 30 (top of p. 91) by using the relation $a_{ij} = \frac{1}{i!j!}g_{ij}$ (using the author's notations) where the latter is obtained by comparing Eq. (A45) with Eq. (3.15) in Ref. 30.

Now, by denoting $r = \sqrt{|w|^2}$, we have

$$2r\frac{\mathrm{d}r}{\mathrm{d}t} = w\frac{\mathrm{d}\overline{w}}{\mathrm{d}t} + \overline{w}\frac{\mathrm{d}w}{\mathrm{d}t} = w\overline{\left(\frac{\mathrm{d}w}{\mathrm{d}t}\right)} + \overline{w}\frac{\mathrm{d}w}{\mathrm{d}t}. \tag{A49}$$

It follows then by using Eq. (A47) that

$$\frac{\mathrm{d}r}{\mathrm{d}t} = \mathrm{Re}(\beta(\lambda))r + \mathrm{Re}(c(\lambda))r^3 + o(r^3). \tag{A50}$$

Note also that by differentiating both sides of $w = r(\cos\theta + \sqrt{-1}\sin\theta)$ and making use of Eqs. (A47) and (A50), we obtain

$$\frac{\mathrm{d}\theta}{\mathrm{d}t} = \mathrm{Im}(\beta(\lambda)) + \mathrm{Im}(c(\lambda))r^2 + o(r^2). \tag{A51}$$

The system (A50) and (A51) is the normal form of Eq. (A45) given by Eq. (A47) rewritten in polar coordinates.

Note that if the conditions given by (A46) hold and $\mathrm{Re}(c(\lambda_c)) \neq 0$, then the planar system (A50) and (A51) admits a Hopf bifurcation at $\lambda = \lambda_c$ (Theorems 3.3 and 3.4 in Ref. 30). Since $\mathrm{Re}(\beta(\lambda))$

> 0 for $\lambda > \lambda_c$ thanks to (A46), one deduces from (A50) that the bifurcation is subcritical when $\mathrm{Re}(c(\lambda_c)) > 0$ and supercritical when $\mathrm{Re}(c(\lambda_c)) < 0$.

Recall also from the normal form theory that Eq. (A45) is topologically equivalent to (A50) and (A51) near the origin (Ref. 30, pp. 89–93). Specifically, to determine the type of bifurcation associated with Eq. (A45), it suffices to determine the sign of $\mathrm{Re}(c(\lambda_c))$. By using (A48), we obtain the following formula for $\mathrm{Re}(c(\lambda_c))$, which is called the first Lyapunov coefficient or the Poincaré–Hopf formula associated with the planar system (A45):

$$\ell_1 = \mathrm{Re}(c(\lambda_c)) = \mathrm{Re}\Big(\frac{a_{20}a_{11}\sqrt{-1}}{\mathrm{Im}(\beta(\lambda_c))} + a_{21}\Big). \tag{A52}$$

To summarize, under the condition (A46), a Hopf bifurcation occurs at $\lambda = \lambda_c$ for the planar system (A45); the bifurcation is subcritical if $\ell_1 > 0$ and supercritical if $\ell_1 < 0$.

Step 2. With the above preparation, we turn now to derive the Stuart–Landau normal form (36) and the first Lyapunov coefficient (40) for the GK system by reducing it onto the leading-order approximation of its two-dimensional center manifold.

Note that thanks to the condition (32) and (33), the center subspace E_c for λ in a sufficiently small neighborhood of λ_c is two-dimensional and is spanned by the eigenvectors associated with $\beta_1(\lambda)$ and $\beta_2(\lambda)$, the eigenvalues forming the eigenpair that crosses the imaginary axis as λ crosses λ_c. We denote by E_s the supplement of E_c in $\mathbb{R}^{Nd}$, i.e., $\mathbb{R}^{Nd} = E_c \oplus E_s$. The reduced equations of the Nd-dimensional GK (28) onto its center manifold is given by

$$\frac{\mathrm{d}z_i}{\mathrm{d}t} = \beta_i(\lambda)z_i + \Big\langle F_N\Big(z_1\boldsymbol{e}_1 + z_2\boldsymbol{e}_2 + \Phi(z_1,z_2)\Big), \boldsymbol{e}_i^*\Big\rangle, \quad i = 1,2, \tag{A53}$$

where $z_i = \langle y_N, \boldsymbol{e}_i^*\rangle$ for $i = 1,2$ and $\Phi : E_c \to E_s$ denotes a center-manifold function. Since the two-dimensional center manifold attracts all the solution trajectories that stay in a sufficiently small neighborhood of the origin (see, e.g., Theorem 2 in Sec. 2.4 of Ref. 71), it suffices to use the reduced system (A53) to characterize the Hopf bifurcation for the original GK system.

Recall that, in Eq. (A53), we have $\beta_2(\lambda) = \overline{\beta_1}(\lambda)$ and $\boldsymbol{e}_2 = \overline{\boldsymbol{e}_1}$. As a result, $z_2 = \overline{z_1}$. In particular, the equation for z_2 is obtained by simply taking the complex conjugate of the equation for z_1. The characterization is thus specified only by using the equation of z_1 (simply denoted by z below),

$$\frac{\mathrm{d}z}{\mathrm{d}t} = \beta_1(\lambda)z + \Big\langle F_N\Big(z\boldsymbol{e}_1 + \bar{z}\boldsymbol{e}_2 + \Phi(z,\bar{z})\Big), \boldsymbol{e}_1^*\Big\rangle. \tag{A54}$$

Assuming the form of F_N given by (34), note that it is sufficient to use the (quadratic) leading-order approximation of Φ in order to determine the first Lyapunov coefficient ℓ_1 given by (A52). This is because higher-order terms in the approximation of Φ contribute to terms of order 4 or higher in the reduced equation (A54) and thus do not contribute to the formula of ℓ_1. To conclude, we use results from the approximation theory of invariant manifolds; see Sec. 2 in Ref. 37. When applied to the present context, these approximation results (Theorem 2 in Ref. 37) show that under the assumption (34) on the nonlinearity F_N and the non-resonance condition (35), the leading-order approximation Φ_2 of Φ is given by

$$\Phi_2(z,\bar{z}) = \sum_{n=3}^{Nd}\Bigg[\frac{\langle F_N^{(2)}(\boldsymbol{e}_1,\boldsymbol{e}_1),\boldsymbol{e}_n^*\rangle}{2\beta_1(\lambda)-\beta_n(\lambda)}z^2 + \frac{\langle F_N^{(2)}(\boldsymbol{e}_2,\boldsymbol{e}_2),\boldsymbol{e}_n^*\rangle}{2\overline{\beta_1}(\lambda)-\beta_n(\lambda)}\bar{z}^2 + \frac{\langle F_N^{(2)}(\boldsymbol{e}_1,\boldsymbol{e}_2),\boldsymbol{e}_n^*\rangle + \langle F_N^{(2)}(\boldsymbol{e}_2,\boldsymbol{e}_1),\boldsymbol{e}_n^*\rangle}{2\mathrm{Re}(\beta_1(\lambda))-\beta_n(\lambda)}z\bar{z}\Bigg]\boldsymbol{e}_n; \tag{A55}$$

cf. Eqs. (2.47) and (2.48) in Ref. 37 with $k = 2$.

By using (34) and the leading-order approximation (A55) of Φ in (A54), we obtain the formulas of the coefficients involved in (A52) for the GK system, and they are given by (38) and (39). The derivation is now complete. □

APPENDIX B: NONLINEAR TERMS IN GK APPROXIMATIONS OF THE KF MODEL FOR THE LYAPUNOV COEFFICIENT CALCULATION

The determination of the Lyapunov coefficient $\ell_1^N(\lambda_c)$ given in (40) requires the determination of inner products involving terms such as $\boldsymbol{F}_N^{(2)}(\boldsymbol{e}_1,\boldsymbol{e}_2)$ and $\boldsymbol{F}_N^{(3)}(\boldsymbol{e}_1,\boldsymbol{e}_2,\boldsymbol{e}_1)$. We detail here such terms for the KF model written under its form (65) (i.e., near criticality), which unlike those given in (74) do not share the same arguments.

In this respect, we specify first the bilinear term $\boldsymbol{F}^{(2)} : \mathbb{R}^2 \times \mathbb{R}^2 \to \mathbb{R}^2$ and the trilinear term $\boldsymbol{F}^{(3)} : \mathbb{R}^2 \times \mathbb{R}^2 \times \mathbb{R}^2 \to \mathbb{R}^2$ of the KF model (65) to be defined, respectively, by

$$\begin{aligned}\boldsymbol{F}^{(2)}(X_1,X_2) &= \begin{pmatrix} -\dfrac{ap_1p_2}{\bar{y}} + \dfrac{2a\bar{x}p_1q_2}{\bar{y}^2} - \dfrac{a\bar{x}^2q_1q_2}{\bar{y}^3} \\ -3d\bar{x}p_1p_2 \end{pmatrix}, \\ \boldsymbol{F}^{(3)}(X_1,X_2,X_3) &= \begin{pmatrix} \dfrac{ap_1p_2q_3}{\bar{y}^2} - \dfrac{2a\bar{x}p_1q_2q_3}{\bar{y}^3} + \dfrac{a\bar{x}^2q_1q_2q_3}{\bar{y}^4} \\ -dp_1p_2p_3 \end{pmatrix},\end{aligned} \tag{B1}$$

with $X_j = (p_j, q_j)$. As explained in the main text, to simplify the notations, when the two arguments of $\boldsymbol{F}^{(2)}$ are the same, i.e., when $(p_1,q_1) = (p_2,q_2) = (p,q)$, we recover the terms $\boldsymbol{F}^{(2)}(p,q)$ and $\boldsymbol{F}^{(3)}(p,q)$ given in (68) and (69), adopting a slight abuse of notation. The same convention applies for the trilinear term.

We turn now to the explicit formula for $\boldsymbol{F}_N^{(2)}(\boldsymbol{x},\boldsymbol{y})$ with $\boldsymbol{x}$ and $\boldsymbol{y}$ in $\mathbb{R}^{2N}$ in the KF's nonlinear terms recalled in (B1). To do so, we introduce

$$p_x = \sum_{n=1}^{N} x_{2n-1}K_{n-1}(-1), \quad q_x = \sum_{n=1}^{N} x_{2n}K_{n-1}(-1) \tag{B2}$$

and

$$p_y = \sum_{n=1}^{N} y_{2n-1}K_{n-1}(-1), \quad q_y = \sum_{n=1}^{N} y_{2n}K_{n-1}(-1). \tag{B3}$$

The bilinear term $\boldsymbol{F}_N^{(2)}(\boldsymbol{x},\boldsymbol{y})$ is then given according to

$$\left[F_N^{(2)}\right]_j(\boldsymbol{x},\boldsymbol{y}) = \begin{cases} \dfrac{1}{\|\mathcal{K}_{(j-1)/2}\|_{\mathcal{E}}^2}\left(-\dfrac{ap_xp_y}{\bar{y}}+\dfrac{2a\bar{x}p_xq_y}{\bar{y}^2}-\dfrac{a\bar{x}^2q_xq_y}{\bar{y}^3}\right) & \text{for } j \text{ odd},\\ -\dfrac{3d\bar{x}p_xp_y}{\|\mathcal{K}_{(j-2)/2}\|_{\mathcal{E}}^2} & \text{for } j \text{ even}. \end{cases} \tag{B4}$$

Similarly, the trilinear term $\boldsymbol{F}_N^{(3)}(\boldsymbol{x},\boldsymbol{y},\boldsymbol{z})$ is given (for any $\boldsymbol{x}$, $\boldsymbol{y}$, and $\boldsymbol{z}$ in $\mathbb{R}^{2N}$) according to

$$\left[F_N^{(3)}\right]_j(\boldsymbol{x},\boldsymbol{y},\boldsymbol{z}) = \begin{cases} \dfrac{1}{\|\mathcal{K}_{(j-1)/2}\|_{\mathcal{E}}^2}\left(\dfrac{ap_xp_yq_z}{\bar{y}^2}-\dfrac{2a\bar{x}p_xq_yq_z}{\bar{y}^3}+\dfrac{a\bar{x}^2q_xq_yq_z}{\bar{y}^4}\right) & \text{for } j \text{ odd},\\ -\dfrac{dp_xp_yp_z}{\|\mathcal{K}_{(j-2)/2}\|_{\mathcal{E}}^2} & \text{for } j \text{ even}, \end{cases} \tag{B5}$$

with (p_z, q_z) defined as in (B2) replacing x by z, therein.

APPENDIX C: NUMERICAL IMPLEMENTATION DETAILS

In this appendix, we provide details about the numerical experiments conducted in this article, including the computation of the Lyapunov coefficient for the KF model (Appendix C 2) and numerical solvers used to integrate the KF model and its GK approximations (Appendix C 3). The reliance on the Matlab solvers as described below is for enhancing the reproducibility of the results by the interested reader.

1. Construction and initialization of the GK systems

We detail below how the GK systems are constructed and initialized; see also Algorithm 1. First, note that the Koornwinder polynomial K_n defined by (A1) admits the following expansion in terms of the Legendre polynomials:

$$K_n(s) = -\sum_{j=0}^{n-1}(2j+1)L_j(s) + (n^2+1)L_n(s), \tag{C1}$$

for $s \in [-1,1]$, $n \in \mathbb{N}$; see Eq. (3.5) in Ref. 26. In particular, by using $L_n(-1) = (-1)^n$, we have

$$\begin{aligned} K_n(-1) &= -\sum_{j=0}^{n-1}(-1)^j(2j+1) + (-1)^n(n^2+1)\\ &= (-1)^n(n^2+n+1). \end{aligned} \tag{C2}$$

We compute $K_n(s)$ at any given s in the interval $[-1,1]$ by using (C1) together with the following three-term recurrence relation for the Legendre polynomials [see, e.g., Sec. 3.3 in Ref. 74]:

$$(n+1)L_{n+1}(s) = (2n+1)sL_n(s) - nL_{n-1}(s), \tag{C3}$$

for $s \in [-1,1]$, $n \geq 1$. Then, the rescaled polynomial K_n^τ defined on $[-\tau,0]$ is determined according to (A10).

The construction of the Nd-dimensional GK systems for a d-dimensional DDE system, such as (45)–(48) for the KTF model and (74)–(76) for the KF model, boils down, for $0 \leq n \leq N-1$, to the computation of $K_n(-1)$ using (C2), the norms $\|\mathcal{K}_n\|_{\mathcal{E}}$ using (A13), and the coefficients $\boldsymbol{a}_n = (a_{n,0},\ldots,a_{n,n-1})$ by solving the algebraic system $\mathbf{T}\boldsymbol{a}_n = \boldsymbol{b}_n$, with the Koornwinder derivative matrix $\mathbf{T}$ and the vector $\boldsymbol{b}_n$ given in (A18).

Given an initial history $\phi : [-\tau,0] \to \mathbb{R}^d$, the initial data $\boldsymbol{y}_0$ for the Nd-dimensional GK system is obtained as follows [cf. (24)]:

$$y_{0,j} = \frac{\langle \Psi, \mathbb{K}_j^\tau\rangle_{\mathcal{H}_d}}{\|\mathbb{K}_j^\tau\|_{\mathcal{H}_d}^2}, \quad j = 1,\ldots,Nd, \tag{C4}$$

where $\boldsymbol{y}_{0,j}$ denotes the jth component of $\boldsymbol{y}_0$, $\Psi = (\phi, \phi(0))$, and the inner product $\langle\cdot,\cdot\rangle_{\mathcal{H}_d}$ is defined by (A21). Recall from (A25) that $\mathbb{K}_j^\tau(\theta) = \left(\mathbf{K}_j^\tau(\theta), \mathbf{K}_j^\tau(0)\right)$. Recall also that for each $j = 1,\ldots,Nd$, the vectorized (rescaled) Koornwinder polynomial $\mathbf{K}_j^\tau$ is given by the sparse vector $\mathbf{K}_j^\tau(\theta) = (0,\ldots,0,K_{j_q}^\tau(\theta),0,\ldots,0)^{\mathrm{T}}$, where the non-zero component is the j_r-th component and the relation between j and the integer pair (j_q, j_r) is given by (A22) and (A23); see (A24). Then, the inner product $\langle\Psi,\mathbb{K}_j^\tau\rangle_{\mathcal{H}_d}$ is reduced to

$$\langle\Psi,\mathbb{K}_j^\tau\rangle_{\mathcal{H}_d} = \langle\Psi_{j_r},\mathcal{K}_{j_q}^\tau\rangle_{\mathcal{H}_1}, \tag{C5}$$

where $\Psi_{j_r} = (\phi_{j_r}, \phi_{j_r}(0))$ with ϕ_{j_r} denoting the j_r-th component of ϕ, $\mathcal{H}_1$ is defined in (A8), the inner product $\langle\cdot,\cdot\rangle_{\mathcal{H}_1}$ is given by (A9), and $\mathcal{K}_j^\tau = (K_j^\tau, K_j^\tau(0))$; cf. (A11). Writing out the inner product on the RHS (C5) using (A9) and by noting that $K_j^\tau(0) = 1$ [cf. (A12)], we get

$$\langle\Psi,\mathbb{K}_j^\tau\rangle_{\mathcal{H}_d} = \frac{1}{\tau}\int_{-\tau}^0 \phi_{j_r}(\theta)K_{j_q}^\tau(\theta)\,\mathrm{d}\theta + \phi_{j_r}(0). \tag{C6}$$

Note also that by (A27) and (A13), we have

$$\begin{aligned} \|\mathbb{K}_j^\tau\|_{\mathcal{H}_d} &= \|\mathcal{K}_{j_q}^\tau\|_{\mathcal{H}_1}\\ &= \|\mathcal{K}_{j_q}\|_{\mathcal{E}} = \sqrt{\frac{(j_q^2+1)((j_q+1)^2+1)}{2j_q+1}}. \end{aligned} \tag{C7}$$

Then, (C4) is reduced to

$$y_{0,j} = C(j)\left(\frac{1}{\tau}\int_{-\tau}^0 \phi_{j_r}(\theta)K_{j_q}^\tau(\theta)\mathrm{d}\theta + \phi_{j_r}(0)\right), \tag{C8}$$

with

$$C(j) = \frac{2j_q+1}{(j_q^2+1)((j_q+1)^2+1)},$$

for $j = 1,\ldots,Nd$. In practice, the integral can be evaluated by any commonly used quadrature rules in which the values of $K_{j_q}^\tau$ at the quadrature points are calculated by using (A10) and (C1). For the numerical experiments we performed, the Romberg's method is used, which uses values on a uniform mesh of $[-\tau,0]$ with 2^m+1 grid points. We have chosen $m = 20$ for our numerical experiments.

2. Calculation of the Lyapunov coefficient

We provide here practical aspects for the good implementation of Algorithm 2. Motivated by applications, we treat here the delay parameter τ as the bifurcation parameter.

1. Forming $\Gamma_N(\tau)$. We form the $Nd \times Nd$ matrix $\Gamma_N(\tau)$ given by (29) treating τ as the bifurcation parameter λ. In that respect, $K_n(-1)$ is evaluated according to (C2).
2. Bisection method to determine τ_c such that $\mathrm{Re}(\beta_1(\tau_c)) = 0$. First, identify an interval $I = [\tau_{\min}, \tau_{\max}]$ that contains τ_c, i.e., with $\mathrm{Re}(\beta_1(\tau_{\max})) > 0$ and $\mathrm{Re}(\beta_1(\tau_{\min})) < 0$. Then, compute eigenvalues of $\Gamma_N(\tau)$ with $\tau = (\tau_{\min} + \tau_{\max})/2$ and redefine $\tau_{\min}$ and $\tau_{\max}$ according to the sign of $\mathrm{Re}(\beta_1(\tau))$. The Matlab built-in function `eigs` is used for determining eigenvalues in our computations. The bisection is continued until the real part of the rightmost eigenvalue $\beta_1(\tau)$ is smaller than a given threshold (set to 10^{-10} for all the experiments conducted), providing thus an estimate of τ_c.
3. Forming the bilinear and trilinear terms. These terms are given explicitly in (B4) and (B5) for the KF model (60). For the KTF model (1), the bilinear term is given by

$$\left[F_N^{(2)}\right]_j(\boldsymbol{x}, \boldsymbol{y}) = -\frac{1}{\mu \|\mathcal{K}_{j-1}\|_{\mathcal{E}}^2} f(\boldsymbol{x}) f(\boldsymbol{y}), \tag{C9}$$

with

$$f(\boldsymbol{x}) = \left(\sum_{n=1}^{N} x_n K_{n-1}(-1)\right).$$

There is no trilinear term for the KTF model.
4. Forming the coefficients a_{20}^N, a_{11}^N, and a_{21}^N in (40). Once τ_c is found, we compute the eigenvalues and eigenvectors $\{(\beta_j, \boldsymbol{e}_j)\}$ of $\Gamma_N(\tau_c)$, on one hand, and the spectral elements, $\{(\beta_j^*, \boldsymbol{e}_j^*)\}$, of its transpose $[\Gamma_N(\tau_c)]^{\mathrm{T}}$, on the other. The eigen elements are indexed in the descending order of the real part of the eigenvalues. For complex conjugate eigenvalues, the one with the positive imaginary part comes first for $\Gamma_N(\tau_c)$ and the one with the negative imaginary part comes first for $[\Gamma_N(\tau_c)]^{\mathrm{T}}$ to ensure orthogonality. To ensure the bi-orthonormality condition $\langle \boldsymbol{e}_j, \boldsymbol{e}_k^* \rangle = \delta_{jk}$, we normalize $\boldsymbol{e}_j^*$ by redefining it to be $\boldsymbol{e}_j^* / \langle \boldsymbol{e}_j, \boldsymbol{e}_j^* \rangle$. The coefficients a_{20}^N, a_{11}^N, and a_{21}^N given by (38) and (39) are then computed by plugging accordingly the dominant eigenvectors $\boldsymbol{e}_1$ or $\boldsymbol{e}_2$ into the arguments of the bilinear and trilinear terms determined in step 3 above. The Lyapunov coefficient $\ell_1^N(\tau_c)$ is then computed according to (40).

3. Numerical solvers and schemes

- *Numerical solver for DDEs.* The integration of the KTF model (1) and the KF model (60) is performed with the Matlab built-in solver `dde23`, which implements a Runge–Kutta method of type (2,3).[75] For a comprehensive treatment of convergence, error estimates, stepsize control, and stability in the numerical solution to DDEs, we refer to Ref. 76.
  For the integration of the KTF model (1) in all the numerical experiments, the following setting in the `dde23`'s `options` argument is used: `options = ddeset("RelTol,"1E-5,"AbsTol,"1E-10,"MaxStep,"1,"InitialStep,"1E-4)`.
  For the integration of the KF model (60) in all the numerical experiments, the following setting in the `dde23`'s `options` argument is used: `options = ddeset("RelTol,"1E-8,"AbsTol,"1E-10,"MaxStep,"1,"InitialStep,"1E-4)`. A larger relative error tolerance is used for the KTF model because the solutions can get much closer to zero than those of the KF model for the parameter regimes considered.
  The solver `dde23` uses adaptive time steps. Thus, after the DDEs are solved, and for visualization purpose, the solutions are evaluated on a uniform mesh with sufficiently fine resolution over either the whole time interval of integration when solution time series is plotted (such as in Fig. 5) or over a time interval located toward the end of the simulation when only the attractor is plotted. This evaluation on a uniform grid is performed with the Matlab built-in interpolation function `deval`. For some experiments as specified below, the GK systems are initialized by projecting the last segment of the DDE solution of length τ onto the Koornwinder basis. The DDE solution's segment over the desired time grid as required by the adopted quadrature rule is also computed using the interpolation routine `deval`; see (C8).
- *Numerical solver for GK systems.* The GK systems for the KF model (60) are integrated with the Matlab built-in solver `ode45`, which implements a Runge–Kutta method of type (4,5). All the GK systems are solved with the following setting in the `ode45`'s `options` argument: `options = odeset("RelTol,"1E-8,"AbsTol,"1E-10,"MaxStep,"1,"InitialStep,"1E-4)`. Like for the DDE solutions explained above, after the GK systems are solved using `ode45`, the solutions are further evaluated over the relevant sub-intervals on fine mesh grids using `deval` for visualization purpose.
- *Numerical scheme for the complex-valued reduced systems of the KTF model.* The two complex-valued reduced systems used in Sec. III B [the CM reduced equation (52) and 2D crude truncation shown in Fig. 3] are integrated using a semi-implicit Euler scheme with the linear part treated implicitly and the nonlinear terms explicitly. The time step size used to produce the numerical results of Sec. III B is $\delta t = \tau/2^{12}$.

4. Complimentary numerical aspects

We discuss hereafter the numerical protocol behind few key figures for better reproducibility of the numerical results.

- For each τ-value shown in Fig. 3 of Sec. III B, the initial history ϕ_0 for the KTF model (1) is given by $\phi(\theta) \equiv 0.5$, for all θ in $[-\tau, 0]$. In each case, the KTF model is integrated over the time interval $[0, 6000]$ using the DDE solver of Appendix C 3. The CM reduced equation (52) and the 2D crude truncation are initialized using a projection of the KTF model's solution over the time window $[5000 - \tau, 5000]$. The projection of the DDE solution segment is made as follows. First, this segment is projected onto the first N Koornwinder polynomials with $N = 10$ to obtain $\boldsymbol{y}_0$; see (C8). Then, $\boldsymbol{y}_0$ is rewritten under the eigenbasis $\{\boldsymbol{e}_1, \ldots, \boldsymbol{e}_n\}$ to obtain $\boldsymbol{z}_0$. Finally, the first two components of $\boldsymbol{z}_0$ provide the initial datum for the CM reduced equation (52) and the 2D crude truncation.

These systems are then integrated ahead for 1000 time units with a time step size of $\delta t = \tau/2^{12}$ to produce Fig. 3.

- For Fig. 5 in Sec. IV B, the initial history $\boldsymbol{\phi}_0$ for the KF model (60) is given by $\boldsymbol{\phi}_0(\theta) \equiv (0.2, 0.5)$, $\theta \in [-\tau, 0]$. The system parameters are those given by (78). The initial datum for the 10D GK approximation is taken to be the projection $\boldsymbol{y}_0$ of $\boldsymbol{\phi}_0$ onto the first 10 Koornwinder polynomials according to (C8).
- Regarding Fig. 13, it is worth pointing out that the solutions converge very slowly toward the stable limit cycle especially for the two smallest τ-values used. To save simulation time, we solve the KF model for the larger τ-value first and use the numerical solution so-obtained at the end of the simulation to initiate the model for the (smaller) τ-value of interest. More precisely, we first simulated the KF model for $\tau = 25.4$. For this τ-value, the initial history is taken to be $\boldsymbol{\phi}_0(\theta) \equiv (381.7227, 40.9459) + 1$, which represents perturbation by one unit of the steady state. The model is integrated over the time window $[0, 4 \times 10^5]$. Then, for the immediate smaller τ-value used, i.e., for $\tau = 25.35$, the initial history $\boldsymbol{\phi}_0(\theta)$ is taken to be $X(t + \theta)$ with $t = 4 \times 10^5$ and $\theta \in [-\tau, 0]$, where X denotes the solution to the KF model for $\tau = 25.4$. The KF model is then integrated for 4×10^5 time units ahead but this time for $\tau = 25.35$. The procedure is repeated for the other smaller τ-values except for $\tau = 25.24$ and $\tau = 25.235$ for which the KF model is, respectively, integrated for 1×10^6 and 4×10^6 time units ahead to ensure the convergence to the respective limit cycle. For each τ-value, the initial datum for the 20D GK approximation is taken to be the projection of the KF model's solution $X(t + \theta)$ with $t = t_f$, where t_f denotes the final time of the corresponding DDE simulation.

REFERENCES

[1] D. E. Gilsinn, in *Delay Differential Equations: Recent Advances and New Directions* (Springer, New York, 2009), pp. 155–202.
[2] T. Faria and L. T. Magalhães, J. Differ. Equations **122**, 181 (1995).
[3] B. Hassard and Y. H. Wan, J. Math. Anal. Appl. **63**, 297 (1978).
[4] B. D. Hassard, N. D. Kazarinoff, and Y. H. Wan, *Theory and Applications of Hopf Bifurcation*, London Mathematical Society Lecture Note Series Vol. 41 (Cambridge University Press, London, 1981).
[5] R. Qesmi, M. Babram, and M. L. Hbid, Appl. Math. Comput. **175**, 932 (2006).
[6] W. Wischert, A. Wunderlin, A. Pelster, M. Olivier, and J. Groslambert, Phys. Rev. E **49**, 203 (1994).
[7] S. N. Chow and J. Mallet-Paret, J. Differ. Equations **26**, 112 (1977).
[8] R. Nussbaum, Trans. Am. Math. Soc. **238**, 139 (1978).
[9] S. A. van Gils, "On a formula for the direction of Hopf bifurcation," Stichting Mathematisch Centrum preprint TW 225/82 (Stichting Mathematisch Centrum, 1982).
[10] H. W. Stech, J. Math. Anal. Appl. **109**, 472 (1985).
[11] S. L. Das and A. Chatterjee, Nonlinear Dyn. **30**, 323 (2002).
[12] A. H. Nayfeh, Nonlinear Dyn. **51**, 483 (2008).
[13] J. K. Hale and S. M. Verduyn Lunel, *Introduction to Functional-Differential Equations*, Applied Mathematical Sciences Vol. 99 (Springer-Verlag, New York, 1993).
[14] O. Diekmann, S. A. Van Gils, S. Lunel, and H.-O. Walther, *Delay Equations: Functional-, Complex-, and Nonlinear Analysis* (Springer Science & Business Media, 2012), Vol. 110.
[15] J. K. Hale, L. T. Magalhães, and W. Oliva, *Dynamics in Infinite Dimensions* (Springer Science & Business Media, 2006), Vol. 47.
[16] N. D. Kazarinoff, Y.-H. Wan, and P. van den Driessche, IMA J. Appl. Math. **21**, 461 (1978).
[17] G. Stépán, Nonlinear Anal. Theory Methods Appl. **10**, 913 (1986).
[18] S. A. Campbell and J. Bélair, Can. Appl. Math. Q **3**, 137 (1995).
[19] E. Stone and S. A. Campbell, J. Nonlinear Sci. **14**, 27 (2004).
[20] S. A. Campbell, in *Delay Differential Equations: Recent Advances and New Directions* (Springer, New York, 2009), pp. 221–244.
[21] K. Engelborghs, T. Luzyanina, and D. Roose, ACM Trans. Math. Softw. **28**, 1 (2002).
[22] J. Sieber, K. Engelborghs, T. Luzyanina, G. Samaey, and D. Roose, "DDE-BIFTOOL manual—Bifurcation analysis of delay differential equations," arXiv:1406.7144 (2004).
[23] B. Wage, see https://dspace.library.uu.nl/handle/1874/296912 for "Normal form computations for Delay Differential Equations in DDE-BIFTOOL," master's thesis (Utrecht University, Utrecht, the Netherlands, 2014).
[24] M. M. Bosschaert, S. G. Janssens, and Y. A. Kuznetsov, SIAM J. Appl. Dyn. Syst. **19**, 252 (2020).
[25] D. Breda, O. Diekmann, M. Gyllenberg, F. Scarabel, and R. Vermiglio, SIAM J. Appl. Dyn. Syst. **15**, 1 (2016).
[26] M. D. Chekroun, M. Ghil, H. Liu, and S. Wang, Disc. Cont. Dyn. Sys. A **36**, 4133 (2016).
[27] T. H. Koornwinder, Can. Math. Bull. **27**, 205 (1984).
[28] M. D. Chekroun, A. Kröner, and H. Liu, in *Hamilton-Jacobi-Bellman Equations. Numerical Methods and Applications in Optimal Control*, edited by D. Kalise, K. Kunisch, and Z. Rao (De Gruyter, 2018), Vol. 21, pp. 61–96.
[29] J. D. Crawford, Rev. Mod. Phys. **63**, 991 (1991).
[30] Y. A. Kuznetsov, *Elements of Applied Bifurcation Theory* (Springer, 1995).
[31] M. D. Chekroun and D. Kondrashov, Chaos **27**, 093110 (2017).
[32] D. Kondrashov, M. D. Chekroun, and P. Berloff, Fluids **3**, 21 (2018).
[33] M. D. Chekroun, A. Tantet, H. A. Dijkstra, and J. D. Neelin, J. Stat. Phys. (published online).
[34] A. Tantet, M. D. Chekroun, J. D. Neelin, and H. A. Dijkstra, J. Stat. Phys. (published online).
[35] A. Tantet, M. D. Chekroun, J. D. Neelin, and H. A. Dijkstra, J. Stat. Phys. (published online).
[36] J. E. Marsden and M. McCracken, *The Hopf Bifurcation and Its Applications*, Applied Mathematical Sciences Vol. 19 (Springer-Verlag, New York, 1976).
[37] M. D. Chekroun, H. Liu, and J. C. McWilliams, J. Stat. Phys. (published online).
[38] L. Roques, M. D. Chekroun, M. Cristofol, S. Soubeyrand, and M. Ghil, Proc. R. Soc. A **470**, 20140349 (2014).
[39] M. Ghil, M. D. Chekroun, and G. Stepan, Proc. R. Soc. A **471**, 20150097 (2015).
[40] A. Keane, B. Krauskopf, and C. M. Postlethwaite, Chaos **27**, 114309 (2017).
[41] N. Boers, M. D. Chekroun, H. Liu, D. Kondrashov, D.-D. Rousseau, A. Svensson, M. Bigler, and M. Ghil, Earth Syst. Dyn. **8**, 1171 (2017).
[42] M. Ghil, I. Zaliapin, and S. Thompson, Nonlinear Process. Geophys. **15**, 417 (2008).
[43] B. Krauskopf and J. Sieber, Proc. R. Soc. A **470**, 20140348 (2014).
[44] A. Keane, B. Krauskopf, and C. Postlethwaite, SIAM J. Appl. Dyn. Syst. **14**, 1229 (2015).
[45] A. Keane, B. Krauskopf, and C. M. Postlethwaite, SIAM J. Appl. Dyn. Syst. **15**, 1656 (2016).
[46] M. Chekroun, M. Ghil, and J. D. Neelin, in *Advances in Nonlinear Geosciences*, edited by A. Tsonis (Springer, 2018), pp. 1–33.
[47] A. Keane, B. Krauskopf, and H. A. Dijkstra, Philos. Trans. R. Soc. A **377**, 20180121 (2019).
[48] V. Kolmanovskii and A. Myshkis, *Introduction to the Theory and Applications of Functional Differential Equations* (Springer Science & Business Media, 2013), Vol. 463.
[49] I. Koren and G. Feingold, Proc. Natl. Acad. Sci. U.S.A. **108**, 12227 (2011).
[50] I. Koren, E. Tziperman, and G. Feingold, Chaos **27**, 013107 (2017).
[51] H. Brézis, *Functional Analysis, Sobolev Spaces and Partial Differential Equations* (Springer, 2010).
[52] R. Curtain and H. Zwart, *An Introduction to Infinite-Dimensional Linear Systems Theory* (Springer, 1995), Vol. 21.
[53] Bypassing efficiently the resolution of the infinite-dimensional Hamilton-Jacobi-Bellman equation associated with the optimal control problem of the original DDE; see Sec. 4.4 of Ref. 28.

[54]The formula (26) appeared in Appendix C of Ref. 26. Appendix A 4 provides details about the derivation of this formula.
[55]The latter approximation corresponds to the minimal dimension required to resolve accurately the dominant eigenpair of the KTF model. We recall that the approximation $h_N(t)$ is obtained according to (10).
[56]J. Guckenheimer and P. Holmes, *Nonlinear Oscillations, Dynamical Systems, and Bifurcations of Vector Fields*, Applied Mathematical Sciences Vol. 42 (Springer-Verlag, New York, 1990).
[57]We mention that these performances may be improved away from criticality by optimized deformations of the CM leading-order approximations; see Secs. 4 and 5 of Ref. 37.
[58]Note that a slight abuse of notation holds here. The term $\boldsymbol{F}^{(2)}$ is indeed presented depending on the dummy variable $X = (p, q)$, but actually, this term is bilinear and in that sense depends not only on X but also on an auxiliary variable $X' = (p', q')$. For instance, its 1st component is given by $\boldsymbol{F}_1^{(2)}(X, X') = -app'/\bar{y} + 2a\bar{x}pq'/\bar{y}^2 - a\bar{x}^2qq'/\bar{y}^3$. However, by making $X = X'$, we recover the 1st component in (68). We have thus opted to denote $\boldsymbol{F}^{(2)}(X, X)$ simply by $\boldsymbol{F}^{(2)}(X)$. Similar remarks hold for the trilinear term $\boldsymbol{F}^{(3)}$. See Appendix B.
[59]K. Gopalsamy, *Stability and Oscillations in Delay Differential Equations of Population Dynamics* (Springer Science & Business Media, 2013), Vol. 74.
[60]Here, this value of the Lyapunov coefficient is obtained for $N = 50$, i.e., by using a 100-dimensional GK approximation.
[61]Our numerical analysis indicates that $a_\#$ lies in between 0.008 648 901 372 385 and 0.008 648901 794 979. The corresponding first four eigenvalues as obtained from a 120D GK approximation are $\beta_1(\tau_c) = 0.000\,000\,000\,000\,921 + i0.002\,886\,405\,353\,469$, $\beta_2(\tau_c) = \overline{\beta_1(\tau_c)}$, $\beta_3(\tau_c) = 0.000\,000\,000\,002\,492 + i0.002\,886\,405\,882\,396$, and $\beta_4(\tau_c) = \overline{\beta_3(\tau_c)}$ and satisfy the characteristic equation (80) of the KF model up to machine precision.
[62]A. Gritsun, Philos. Trans. R. Soc. A **371**, 20120336 (2013).
[63]O. Pujol and A. Jensen, Physica D **399**, 86 (2019).
[64]Figure 1 of Ref. 63 predicts a steady state whose $\bar{x}$-component (H) is zero, which is excluded due to (62) when b and c are non-zero.
[65]S. Busenberg and P. van den Driessche, J. Math. Anal. Appl. **172**, 463 (1993).
[66]That is, a non-self-intersecting continuous loop in the plane, a loop being the image in the plane by a continuous function γ of an interval I (say [0, 1]) such that $\gamma(0) = \gamma(1)$.
[67]A. Koseska, E. Volkov, and J. Kurths, Phys. Rep. **531**, 173 (2013).
[68]X. Han, M. Wei, Q. Bi, and J. Kurths, Phys. Rev. E **97**, 012202 (2018).
[69]D. Rosenfeld, Y. Kaufman, and I. Koren, Atmos. Chem. Phys. **6**, 2503 (2006).
[70]G. Feingold, I. Koren, T. Yamaguchi, and J. Kazil, "On the reversibility of transitions between closed and open cellular convection," Atmos. Chem. Phys. **15**, 7351 (2015).
[71]J. Carr, *Applications of Centre Manifold Theory*, Applied Mathematical Sciences Vol. 35 (Springer-Verlag, New York, 1981), pp. vi+142.
[72]T. Ma and S. Wang, *Bifurcation Theory and Applications*, World Scientific Series on Nonlinear Science. Series A: Monographs and Treatises Vol. 53 (World Scientific Publishing Co. Pte. Ltd., Hackensack, NJ, 2005), pp. xiv+375.
[73]T. Ma and S. Wang, *Phase Transition Dynamics* (Springer, 2014).
[74]J. Shen, T. Tang, and L.-L. Wang, *Spectral Methods: Algorithms, Analysis and Applications*, Springer Series in Computational Mathematics Vol. 41 (Springer, Heidelberg, 2011).
[75]L. F. Shampine and S. Thompson, Appl. Numer. Math. **37**, 441 (2001).
[76]A. Bellen and M. Zennaro, *Numerical Methods for Delay Differential Equations*, Numerical Mathematics and Scientific Computation (Oxford University Press, 2013).